Extracellular vesicles stimulate smooth muscle cell migration by presenting collagen VI.

Alexander Kapustin[1*], Sofia Serena Tsakali[1], Meredith Whitehead[1], George Chennell[2], Meng-Ying Wu[1], Chris Molenaar[1], Anton Kutikhin[3], Leo Bogdanov[3], Maxim Sinitsky[3], Kseniya Rubina[4], Aled Clayton[5], Frederik J Verweij[6], Dirk Michiel Pegtel[7], Simona Zingaro[8], Arseniy Lobov[9], Bozhana Zainullina[10], Dylan Owen[11], Maddy Parsons[8], Richard E. Cheney[12], Derek Warren[13], Martin James Humphries[14], Thomas Iskratsch[15], Mark Holt[7], and Catherine M Shanahan[1*]

[1] School of Cardiovascular and Metabolic Medicine & Sciences, James Black Centre, King's College London, 125 Coldharbour Lane, London, SE5 9NU, UK, Tel. 020 7848 5221, FAX 020 7848 5193,

[2]Wohl Cellular Imaging Centre, King's College London, 5 Cutcombe Road, London, SE5 9NU

[3]Laboratory for Molecular, Translational and Digital Medicine, Research Institute for Complex Issues of Cardiovascular Diseases, 6 Sosnovy Boulevard, Kemerovo, 650002, Russian Federation

[4] Laboratory of Morphogenesis and Tissue Reparation, Faculty of Medicine, Lomonosov Moscow State University, Lomonosovsky av. 27-1, Moscow, 119991, Russia, tel/fax +74959329904

[5]Tissue Microenvironment Research Group, Division of Cancer & Genetics, School of Medicine, Cardiff University, Tenovus Building, Cardiff, UK, CF14 2XN

[6]Division of Cell Biology, Neurobiology & Biophysics, Utrecht University, Padualaan 8, 3584 CH, Utrecht, The Netherlands

[7]Amsterdam UMC, Location Vrije Universiteit Amsterdam, Department of Pathology, Cancer Center Amsterdam, De Boelelaan 1117, Amsterdam, The Netherlands

[8]Randall Centre for Cell and Molecular Biophysics, School of Basic and Medical Biosciences, King's College London, New Hunt's House, Guy's Campus, London, SE1 1UL UK.

[9]Laboratory of Regenerative Biomedicine, Institute of Cytology of the Russian Academy of Sciences, 4 Tikhoretskiy Prospekt, 194064, St. Petersburg, Russia

[10]Centre for Molecular and Cell Technologies, Research Park, St. Petersburg State University, 7/9 Universitetskaya Embankment, 199034, St. Petersburg, Russia

[11]Institute of Immunology and Immunotherapy, School of Mathematics and Centre of Membrane Proteins and Receptors (COMPARE), University of Birmingham, Birmingham, B15 2TT, UK.

[12]Department of Cell Biology and Physiology, School of Medicine, University of North Carolina at Chapel Hill, Chapel Hill, NC 27599, USA

[13]School of Pharmacy, University of East Anglia, Norwich Research Park, Norwich, Norfolk, UK, NR4 7TJ

[14]Wellcome Centre for Cell-Matrix Research, Faculty of Biology, Medicine & Health, Manchester Academic Health Science Centre, University of Manchester, Michael Smith Building, Oxford Road, Manchester, M13 9PT, United Kingdom

[15]School of Engineering and Materials Science, Faculty of Science and Engineering, Queen Mary University of London, Engineering Building, Mile End Road, E1 4NS

* Corresponding authors

Email: Alexander.kapustin@kcl.ac.uk

Email: Cathy.shanahan@kcl.ac.uk

Words: small extracellular vesicles, cell adhesion, vascular remodelling

Abstract

The extracellular matrix (ECM) supports blood vessel architecture and functionality and undergoes active remodelling during vascular repair and atherogenesis. Vascular smooth muscle cells (VSMCs) are essential for vessel repair and, via their secretome, are able to invade from the vessel media into the intima to mediate ECM remodelling. Accumulation of fibronectin (FN) is a hallmark of early vascular repair and atherosclerosis and here we show that FN stimulates VSMCs to secrete small extracellular vesicles (sEVs) by activating the β1 integrin/FAK/Src pathway as well as Arp2/3-dependent branching of the actin cytoskeleton. Spatially, sEV were secreted via filopodia-like cellular protrusions at the leading edge of migrating cells. We found that sEVs are trapped by the ECM *in vitro* and colocalise with FN in symptomatic atherosclerotic plaques *in vivo*. Functionally, ECM-trapped sEVs induced the formation of focal adhesions (FA) with enhanced pulling forces at the cellular periphery. Proteomic and GO pathway analysis revealed that VSMC-derived sEVs display a cell adhesion signature and are specifically enriched with collagen VI. *In vitro* assays identified collagen VI as playing the key role in cell adhesion and invasion. Taken together our data suggests that the accumulation of FN is a key early event in vessel repair acting to promote secretion of collage VI enriched sEVs by VSMCs. These sEVs stimulate migration and invasion by triggering peripheral focal adhesion formation and actomyosin contraction to exert sufficient traction forces to enable VSMC movement within the complex vascular ECM network.

Introduction.

The healthy arterial vasculature is dominated by a highly organised medial extracellular matrix (ECM) containing organised layers of contractile vascular smooth muscle cells (VSMCs). Vascular pathologies such as atherosclerosis are associated with dramatic remodelling of the ECM ultimately leading to plaque rupture and myocardial infarction or stroke[1]. Progenitor medial VSMCs are essential for vessel repair and must invade through the ECM to form the protective intimal fibrous cap in the plaque. This process of VSMC invasion actively contributes to ECM remodelling[2-4]. The accumulation of liver-derived fibronectin (FN) in the vasculature is an early biomarker of atherosclerotic plaque formation and conditional FN knockout in the liver blocked VSMC invasion and fibrous cap formation in the ApoE mouse model. This suggests that FN is an essential signal for VSMC recruitment and invasion during vascular repair, yet its exact role remains unknown[5-7].

FN has been shown to play key signalling roles by modulating cellular spreading, adhesion, invasion, differentiation and viability during both developmental and pathological processes[8]. Cell adhesion to FN is primarily mediated by α5β1 integrins and proteoglycans acting together to activate small GTP-binding proteins, Cdc42, Rac1, and Rho which in turn induce branched actin cytoskeletal rearrangements to form cellular membrane protrusions, filopodia and lamellipodia, which are attached to the ECM via transient peripheral focal complexes[8-11]. In turn, maturation of focal complexes into focal adhesions (FAs) anchors cytoplasmic actin stress fibers to the ECM and actin polymerisation and actomyosin-mediated contractility generate the traction forces required for cell body locomotion[12, 13].

Exosome-like small extracellular vesicles (sEVs) are novel, cell-matrix crosstalk entities that decorate the ECM and form “migration paths” for tumour cells by enhancing cell adhesion, motility and directionality[14-17]. Mechanistically, sEVs are secreted at the cellular leading edge and promote FA formation by presenting fibronectin (FN)[14, 15, 18, 19]. In addition, sEVs can stimulate motility of immune cells and *Dictyostelium discoideum* by presenting cytokines and/or generating chemoattractants[20-22]. We recently showed that FN is also enriched in VSMC-derived sEVs but the exact role of sEVs in VSMC migration and invasion within the ECM meshwork environment of the vasculature remains unexplored[23].

Here we report that FN in the ECM induces polarized sEV secretion via filopodia by upregulating β1 integrin/FAK/Src and Arp2/3-dependent branched actin pathways. In turn, sEVs promote VSMC migration in a 2D model and enhanced directed cell invasion in a 3D model. Mechanistically sEVs induced formation of focal adhesions (FA) with enhanced pulling forces at the cellular periphery thus switching the leading edge from protrusion activity into contractile mode to enable cell body propulsion. Importantly, we found that that the sEV cargo, collagen VI, is indispensable for triggering FA formation and directed cell invasion. We hypothesize that sEV-triggered peripheral FA formation anchors the cellular leading edge and activates cell contraction to exert sufficient force to allow VSMC invasion into the complex ECM fiber meshwork. This novel mechanism opens a unique therapeutic opportunity to target specifically VSMC invasion activity during vascular repair and restenosis.

Results.

1. ECM components involved in vessel injury repair stimulate sEV release via b1 integrins.

FN is detectable in the vasculature as early as the fatty streak stage and preceding major atherogenic alterations such as neointima formation and it is also a novel marker for symptomatic carotid plaques[5-7]. Given its presence during early stages of vessel injury we hypothesized that FN may modulate sEV secretion to enable vessel repair. FN is secreted as a monomeric protein forming fibrils upon cellular binding so we compared the effects of monomeric FN with the effects of FN immobilised on tissue culture plates to mimic FN fibrils[8]. Plating VSMCs on immobilised FN increased the release of CD63+/CD81+ sEVs 3.5±0.6 fold whilst addition of soluble FN had no effect on EV secretion as detected by CD63-bead capture assay (Fig. 1A). Fibrillar collagen I but not a non-fibrillar laminin also stimulated secretion of CD63+/CD81+ sEVs by VSMCs to the same extent as FN (Fig. S1A).

We next tested if the native VSMC-derived 3D matrix that contains FN and collagen could modulate sEV secretion[24]. VSMCs were induced to produce ECM, cells were removed and fresh VSMCs plated onto these 3D matrices. VSMCs acquired an elongated shape (Figs. 1B and 1C) which is typical for mesenchymal cells in a 3D environment[24] and increased secretion of CD63+/CD81+ sEVs compared to VSMCs plated onto the non-coated plastic (Fig 1D). We observed no changes in the size distribution of sEVs secreted by VSMCs plated either on plastic or FN matrix as detected using Nanoparticle Tracking Analysis (NTA) (Fig 1E). To further characterise the EV populations released western blotting confirmed that sEVs isolated in both conditions were loaded with similar levels of FN and the sEV-specific markers CD63 and Syntenin-1 and lacked the EV-specific marker, α-actinin-4 (Fig 1F)[25]. In addition, treatment of the cells plated onto the matrix with sphingomyelin phosphodiesterase 3 inhibitor (3-O-Methyl-Sphingomyelin, 3-OMS) revealed that CD63+/CD81+ sEV secretion in response to collagen and FN was regulated by sphingomyelin phosphodiesterase 3 (Fig S1B) which regulates sEV generation in multivesicular bodies[26]. Hence, FN triggers secretion of CD63+/CD81+ sEVs, most likely with a late endosomal origin.

Both collagen I and FN are ECM ligands that bind and transduce intracellular signalling via β1 integrin. Therefore, we explored the effect of β1 integrin activating (12G10) or inhibiting antibodies (4B4) on FN-stimulated secretion of CD63+/CD81+ sEVs. Activation of β1 integrin using 12G10 antibody in VSMCs enhanced the effect of FN on sEV secretion (Fig 1G). Inhibition of β1 integrin using the 4B4 antibody blocked CD63+/CD81+ sEV secretion by VSMCs plated on FN (Fig. 1G). Next, we tested the role of the β1 integrin downstream signalling mediators, FAK and Src[27]. Blocking these pathways with small inhibitors (FAM14 and PP2, respectively) reduced sEV secretion by cells plated on FN but not on plastic (Figs. 1H and 1I). Taken together these data suggest that FN matrices stimulate secretion of CD63+/CD81+ sEVs via the β1 integrin signalling pathway.

2. sEV secretion depends on the branched actin cytoskeleton and occurs via filopodia

As β1 integrin regulates the actin cytoskeleton we next tested whether the actin cytoskeleton contributes to FN-induced sEV secretion. Filopodia are finger-like extensions of the plasma membrane that contain a core of bundled actin filaments and these structures play key roles in ECM sensing and cellular invasion[28]. To examine the contribution of filopodia to sEV secretion we treated VSMCs with the formin inhibitor, SMIFH2 that blocks filopodia formation. Inhibition of filopodia formation reduced sEV secretion by VSMCs plated on FN but not plastic indicating this was a specific mechanism stimulated by FN (Fig. 2A). In addition to formins, regulators of branched actin filaments,

Cortactin and Arp2/3, have been implicated in filopodia formation and sEV secretion by tumour cells [18, 29, 30]. Inhibition of Arp2/3 using the drug CK666 reduced sEV secretion both in VSMCs plated on plastic and FN matrix (Fig. 2B). Branched actin is involved in sEV secretion by regulating the docking of multivesicular bodies to the plasma membrane in tumour cells[30]. To understand the role of branched actin in sEV secretion in VSMCs we explored the spatial distribution of sEV secretion by VSMCs using CD63-pHluorin where fluorescence is only observed upon the fusion of MVBs with the plasma membrane[31]. We observed the typical "burst"-like appearance of sEV secretion at the cell-ECM interface (Fig S2A and Supplementary Video S1). Notably, we also observed an intense CD63-pHluorin staining along filopodia-like structures indicating that sEV release can occur in filopodia (Fig S2A and Supplemental Video S1). To test whether MVBs are delivered to filopodia, we stained VSMCs for the filopodia marker, Myosin-10 (Myo10)[32] and observed the presence of endogenous CD63+ MVBs along the Myo10-positive filopodia (Fig. 2C, arrows). Filopodia have been implicated in sEV capture and delivery to endocytosis "hot-spots"[33], so next we examined the directionality of CD63+ MVB movement in filopodia by overexpressing Myo10-GFP and CD63-RFP in live VSMCs. Importantly, we observed anterograde MVB transport toward the filopodia tip (Fig. 2D and Supplemental Video S2) indicative of MVB's secretion.

To test the functional role of Arp2/3 in the sEV secretion pathway, we overexpressed the Arp2/3 subunit, ARPC2-GFP and the F-actin marker, F-tractin-RFP in live VSMCs. As expected, Arp2/3 and F-actin formed a distinct lamellipodia scaffold (Fig. S2B and Supplementary Video S3). We also observed Arp2/3 and F-actin positive vesicle movement through the VSMC cytoplasm (Fig. S2B, arrow, and Supplementary Video S3) suggesting that Arp2/3-driven actin comet tails are involved in intracellular trafficking. Indeed, intracellular parasites engage Arp2/3-driven actin comet tails for propulsion through the cell cytosol and to spread through the cellular filopodia to neighbouring cells[34, 35]. Therefore, we tested if Arp2/3-driven actin comet tails propel MVBs through the cell. To do this we expressed CD63-GFP in live VSMCs to label MVBs and observed MVB propulsion by the F-actin tail (Fig. 2E and Supplementary Video S4).

Altogether these data show that activation of a β1 integrin-specific pathway by the FN matrix induces sEV secretion by VSMCs. Spatially, sEV secretion occurs at VSMC filopodia-like protrusion sites and is assisted by the branched actin network suggesting that sEVs may be tightly involved in the regulation of cell motility and invasion.

3. sEVs are trapped in ECM In Vitro and in atherosclerotic plaque.

EV trapping in the ECM is a prominent feature of the vessel media and intima and EVs become more abundant in the ECM with ageing and disease[36]. Therefore, we next set out to determine if sEV can be trapped in the native matrix *in vitro*. VSMCs were plated on plastic or FN for 24hours and sEVs were visualised by CD63 immunofluorescence. We observed CD63 puncta in close proximity to filopodia-like cell projectiles (Fig 3A). Interestingly, these CD63+ sEVs were observed both on the plastic and FN-coated plates suggesting that sEVs can bind to ECM secreted by VSMCs over the 24h incubation. We also visualised CD63+ sEV trapping in the native ECM produced by VSMCs over a 7 day period and their reduction/absence from the matrix when VSMCs were treated with SMPD3 siRNA (Fig S3).

To understand how VSMCs interact with sEVs in the ECM we next isolated and fluorescently-labelled sEVs and added them to VSMCs to track sEV distribution. Super-resolution microscopy (iSIM) revealed that the addition of sEVs to the cell media resulted in fast uptake by VSMCs and their localization at the nuclear periphery (Fig 3B and Fig S3B). This was particularly obvious in 3D projections (Fig S3B). Next, sEVs were added to FN-coated plates prior to the addition of VSMCs.

This resulted in the sEVs remaining evenly deposited across the ECM and these immobilised EVs were not internalised by cells even after incubation for 24h (Fig 3C and Fig S3C). Notably, no perinuclear localisation of sEVs was observed.

To spatially map the accumulation of sEV markers in the atherosclerotic plaque *in vivo* we collected 12 carotid atherosclerotic plaques and adjacent intact vascular segments excised during carotid endarterectomy. Unbiased proteomics analysis confirmed considerable differences between these 2 sample groups, revealing 213 plaque-specific and 111 intact arterial-specific proteins (Fig 4A and Fig 4B, Tables S1-S5). Differential expression analysis identified 46 proteins significantly overexpressed (fold change ≥ 2 and FDR-adjusted P value ≤ 0.05) in plaques and 13 proteins significantly upregulated in the intact arterial segments (Fig 4C, Table S3). Among the top proteins differentially expressed in plaques were catalytic lipid-associated bioscavenger paraoxonase 1, atherogenic apolipoprotein B-100, HDL-associated apolipoprotein D, iron-associated protein haptoglobin, and inflammation-related matrix metalloproteinase-9 (Table S3). These proteins have previously been implicated in lipid metabolism alterations as well as inflammation in the plaque hence indicating the advanced atherosclerotic plaque signature of the analysed samples. Comparison of the differentially expressed proteins also revealed an accumulation in atherosclerotic regions of fetuin-A (Alpha-2-HS-glycoprotein, P02765, 2.7 fold increase, p=0.003869659), an abundant sEV cargo protein which is recycled by VSMCs. Likewise, the level of another sEV cargo, Apolipoprotein B-100 (P04114) was also significantly elevated (2.8 fold increase, p= 0.000124446) in atherosclerotic plaque (Table S2)[23]. Notably, a negative regulator of sEV secretion, Coronin 1C (Q9ULV4) was downregulated in the plaque (0.6 fold decrease, p=0.000805372, Table S2) consistent with previous studies that suggest sEV secretion is upregulated during plaque progression[36, 37].

To test if FN associates with sEV markers in atherosclerosis, we investigated the spatial association of FN with sEV markers using the sEV-specific marker CD81. Interestingly, FN accumulated both in the neointima and the tunica media where it was significantly colocalised with CD81 (Fig. 4E, 4F and 4G). Notably CD81 and FN colocalization was particularly prominent in cell-free, matrix-rich plaque regions (Figs. 4F and 4G). Western blot analysis confirmed FN accumulation in the plaque region (Figs 4G, S4A, S4B). To understand the origin of plaque FN we performed RT-PCR. FN expression could not be detected in plaques nor in intact vessels, although it was abundant in the liver (*data not shown*), suggesting that the circulation is a key source of FN in atherosclerotic plaques. To test whether circulating FN can be recycled in sEVs and subsequently deposited we treated primary human aortic VSMCs with FN and found that it was endocytosed and subsequently delivered to early and late endosomes together with fetuin A, another abundant sEV cargo elevated in plaques (Figs S4C and S4D). In addition, FN could be co-purified with sEVs from VSMC conditioned media (Fig S4E) and detected on the surface of sEVs by flow cytometry confirming its loading in, and secretion via, sEVs (Fig 4H).

4. sEVs stimulate VSMC migration and invasion and induce peripheral focal adhesions with enhanced pulling force at the leading edge.

FN as a cargo in sEVs promotes FA formation in tumour cells and increases cell speed[14, 15]. As we found that FN is loaded into VSMC-derived sEVs we hypothesized that ECM-entrapped sEVs can enhance cell migration by increasing cell adhesion and FA formation in the context of a FN-rich ECM. Therefore, we tested the effect of sEV deposition onto the FN matrix on VSMC migration in 2D and 3D models. We found that FN coating and the addition of sEVs promoted VSMC velocity and overall migration distance in a 2D single-cell migration model (Figs. 5A, 5B) in agreement with previous studies using tumour cells[14, 15]. In contrast, inhibition of sEV release with 3-OMS had the opposite effect on VSMC velocity and overall migration distance (Figs. 5A, 5B).

To assess the effect of sEVs on cell directionality we exploited a 3D model developed by Sung et al[15] and examined VSMC invasion using a μ-Slide Chemotaxis assay where cells were embedded into FN-enriched 3D Matrigel matrices in the absence or presence of exogenously-added sEVs (Fig. 5C). We developed a script to automatically measure cell invasion parameters (track length, cell speed, straightness, accumulated distance, lateral and vertical displacement and parallel forward motion index (FMI)). The addition of sEVs had no effect on cell speed, accumulated distance or straightness (Figs. 5D, 5E, 5F). However, VSMCs invading in the presence of embedded sEVs migrated more aligned to the FBS gradient compared to cells plated in the absence of sEVs. To test whether this was a feature of all EV populations we also performed the experiment in the presence of larger EVs pelleted at the 10,000x*g* centrifugation step and observed no effect suggesting this mechanism was specific to sEVs (Figs. 5G and 5H).

We wondered whether it was the FN cargo in sEVs that was promoting VSMC migration by enhancing FA assembly and cellular adhesion to FN similar to sEV in cancer cells[14]. Therefore, we measured VSMC adhesion to FN using an adhesion assay where sEVs were added to FN-coated plates and cells were plated onto these matrices for 1h and firmly attached cells counted. Surprisingly we observed a marked reduction of VSMC adhesion to FN in the presence of sEVs (Fig 6A) suggesting that sEV can impair VSMC adhesion. Mesenchymal cell attachment to the matrix is mediated by transient focal complexes present in the cellular protrusion as well as centripetal FAs that link the cellular cytoskeleton to the matrix[12, 13]. Consistent with this we observed both focal complexes in the cellular protrusion as well as more centripetal FAs associated with mature actin stress fibres in VSMCs on FN matrix (Fig S5A). Therefore, we used a live cell spreading assay to monitor cellular adhesion over time using ACEA's xCELLigence. As expected, FN alone stimulated VSMC spreading and adhesion (Figs. 6B and 6C). Addition of sEVs did not impact cellular adhesion over the first ~15 min but then the adhesion was stalled in the presence of sEVs (Fig 6B and 6C) suggesting some defect in further cellular spreading. Again, to test whether this was specific for the sEV subset, we also tested the effect of larger EVs pelleted at 10,000x *g* and found that these EVs had no effect on VSMC adhesion and spreading onto the FN matrix (Fig 6B and 6C). To interrogate the stalling event induced by sEVs in VSMCs we plated cells and counted the number of FAs, average size as well as distance from the cell periphery after 30 mins using TIRF microscopy. Once again plating VSMCs onto FN increased the cell size, number of FAs as well as the number of centripetal FAs as compared to cells spreading over non-coated plastic (Figs 6E-I). Importantly, addition of sEVs to FN significantly reduced the number of FAs and the newly formed FAs were formed in close proximity to the cell periphery (Figs. 6E and 6F). Interestingly, the average FA size was similar between the various conditions (Fig 5I).

Cellular traction force is generated by the FA gradient upon FA turnover - formation at the leading edge and disassembly at the tail[12, 13, 38]. To test if sEVs can influence FA turnover in migrating VSMCs we examined FA turnover in the presence of sEVs. Adhesion sites were visualised by paxillin-RFP reporter expression and the FA turnover index was calculated by counting FA overlap over time using a previously developed algorithm to track individual focal adhesions (Fig S5B)[39]. Interestingly, the FA turnover index remains the same in the presence of sEVs indicating that FA stability was not altered (6J). These data correlate well with no changes observed in FA average size across various conditions (Fig 6I) and indicate that sEVs are not influencing FA assembly or "life-cycle" directly. Rho-dependent activation of actomyosin contractility stabilises FAs by mechanical forces halting fibroblast spreading onto FN[40, 41]. We hypothesized that sEVs trigger the appearance of pre-mature, peripheral FAs by activating Rho-dependent cellular contractility. To test whether sEVs can modulate mature FA contractility we measured individual traction force which is generated by mature adhesion sites in the absence or presence of sEVs (Fig. S5C). VSMCs transfected with paxillin-

RFP were plated on FN and sEV-covered PDMS pillars and pillar displacements were calculated as previously described[42-44]. Importantly, the traction force was increased in the presence of sEVs (Fig 6K). Altogether these data suggest that sEVs can trigger the formation of FAs with enhanced pulling force at the cell periphery.

5. The sEV cargo Collagen VI regulates focal adhesion formation in VSMCs

To identify the components triggering peripheral FA formation we compared the proteomic composition of sEVs with the larger EV fraction, which had no effect on FA formation. We identified 257 proteins in sEVs and 168 proteins in EVs with 142 proteins common between both datasets (Fig 7A, Tables S6-S8, Fig S6A). Functional enrichment analysis revealed that the top 5 clusters were related to cell migration - ECM organization, movement of cell or subcellular component, cell adhesion, leukocyte migration and cell-cell adhesion (Fig 7B, Fig S6B, Table S8). The cell adhesion cluster included collagen VI (chains COL1A1, COL6A2 and COL6A3), extracellular matrix glycoproteins (FN and thrombospondin, THBS2, THBS1) as well as EGF-like repeat and discoidin I-like domain-containing protein (EDIL3) and transforming growth factor-beta-induced protein ig-h3 (TGFBI) (Fig 7B, Fig S6B, Table S8). Notably, these sEV proteins are predominantly involved in cell-matrix interactions and cellular adhesion. LG3BP which regulates cell motility was also presented exclusively in sEVs (Table S6). These cell adhesion modulating proteins including Collagen VI, TGFBI, EDIL and LG3BP were either uniquely or highly enriched in sEVs compared to larger EVs as detected by western blotting (Fig 7C).

Collagen VI was the most abundant protein in VSMC-derived sEVs (Fig 7B, Table S7). Collagen VI was previously implicated in the interaction with the proteoglycan NG2[45] and suppression of cell spreading on FN[46]. To test the role of collagen VI in sEV-induced changes in VSMC spreading we incubated FN-deposited sEVs with an anti-collagen VI antibody to block its interaction with the proteoglycan NG2[47]. Addition of the anti-collagen VI antibody restored VSMC spreading on the FN matrix as compared to non-specific IgG treatment (Fig. 7D). Moreover, sEVs isolated from VSMCs after collagen VI knockdown using siRNA had no effect in the 3D invasion model on cell speed (Fig 7E) or direction (Fig. 7F) but reduced cell alignment to the gradient as compared to VSMCs treated with a scrambled siRNA control (Fig. 7J). Finally, we compared the expression of collagen VI, EDIL3 and TGFBI between the plaque and control aorta tissues (Table S1). Importantly, collagen VI and TGFBI expression were significantly elevated in the plaque (Fig 7I) consistent with increased deposition of sEVs during disease progression. Altogether these data indicate that sEVs induce a reduction in cell spreading and premature peripheral FA formation by presenting collagen VI thus acting to enhance cell locomotion (Graphical Abstract).

Discussion.

VSMC migration and invasion to the site of vascular injury is crucial for vessel repair as well as the pathogenic development of atherosclerotic plaque, however the mechanisms of effective invasion through the complex vascular ECM meshwork have been poorly studied. Here we show that FN, a novel marker of unstable plaques[6], enables VSMC migration and invasion by stimulating secretion of collagen VI-loaded sEVs which decorate the ECM and stimulate FA maturation. Notably, our data are consistent and extend previous reports showed that EV secretion by tumour cells enhances nascent adhesion formation hence facilitating tumor cell migration and invasion[14-16]. In particular, we found that sEVs induce formation of FAs with an enhanced pulling force at the cell periphery thus favouring actomyosin-mediated contractility which is essential for cell body propulsion and locomotion.

Mesenchymal cell migration begins with protrusive activity at the leading edge followed by the forward movement of the cell body[13, 41, 48]. Cell directionality is guided via the integrin β1 "probe" on the tip of cellular protrusions, filopodia and lamellipodia[49]. Cellular protrusions are attached to the ECM via focal complexes and extended by the physical force generated by the branched network of actin filaments beneath the plasma membrane[50]. Focal complexes either disassemble or mature into the elongated centripetally located focal adhesions[40]. These focal adhesions anchor the ECM to actin stress fibres and the traction force generated by actomyosin-mediated contractility pulls the FAs rearward and the cell body forward[12, 13]. Here we report that β1 integrin activation triggers sEV release via the filopodia and sEVs stimulate VSMC migration and invasion in 2D and 3D assays, respectively. To gain insight into how sEVs can stimulate cell motility we explored VSMC protrusive activity using live cell spreading assays and TIRF imaging. FN stimulated VSMC spreading by increasing the number of FAs, which were formed centripetally from the cell plasma membrane. FN decoration with sEV dramatically ceased VSMC spreading by inducing pre-mature formation of FAs at the cellular periphery. Cellular spreading and adhesion are orchestrated by the Rho family of small GTPases, Cdc42, Rac1 and Rho with Cdc42 and Rac1 modulating filopodia and lamellipodia and focal complex formation and Rho controlling FA maturation and actomyosin-mediated contractility[11, 51, 52]. Interestingly, in fibroblasts Rho is specifically degraded in cellular protrusions and cellular spreading on FN is accompanied by transient Rho suppression during the fast cell spreading phase[41, 53, 54]. This phase is followed by Rho activation leading to formation of actin stress fibres, tension increase on the focal complexes and their maturation into elongated centripetally located FAs[40, 41, 53, 55]. Excessive Rho activation leads to premature FA assembly and stress fiber formation resulting in reduced cellular protrusions, inhibition of cellular spreading and motility on the FN matrix[41, 53, 56-58] Altogether these data indicate that Rho activity, in mesenchymal cells with extensive FA networks such as fibroblasts or VSMCs, can slow down cell migration by immobilising cells[13]. However, we found that sEVs are not influencing mature FA stability. On the contrary, sEV-induced FAs were spatially restricted to the cell periphery near cellular protrusions and were characterised by an enhanced pulling force activity. Interestingly, fibroblast polarization is driven by Smurf1-dependent RhoA ubiquitinylation and localised degradation in cellular protrusions[54]. A recent study indicated that Rho-dependent contractility is essential for cell invasion in a 3D model and it is tempting to speculate that local Rho activity can enable VSMC invasion by stabilizing FAs at the leading edge and stimulating actomyosin-mediated contractility and cell body movement[59]. On the other hand Rho–ROCK activity is critical for the protease-independent rounded motility of tumour cells and cell types with few adhesion contacts (ameboid) when Rho-dependent contractile forces generate hydrostatic pressure forming multiple membrane blebs to invade the ECM[60, 61]. In fact, we observed an extensive secretion of sEVs which ceased protrusion activity; also VSMCs acquired a rounded morphology when "hovering" over the FN matrix decorated with sEVs (data not shown). Hence, it will be

interesting to study in the future if VSMCs can "high-jack" some elements of "amoeboid-like invasiveness" mode seen in tumors by secreting sEVs.

Collagen VI is a nonfibrillar collagen that assembles into beaded microfilaments upon secretion and it plays both structural and signalling roles[62]. Interestingly, type VI collagen deposition by interstitial fibroblasts is increased in the infarcted myocardium and collagen VI knockout in mice improves cardiac function, structure and remodelling after myocardial infarction via unknown pathways[63, 64]. Immunohistochemical analysis showed that in the healthy vasculature collagen VI is detected in the endothelial basement membrane in the intima and is also forms fibrillar structures between smooth muscle cells in the media. In the fibrous plaque collagen VI is diffusely distributed throughout both the fibrous cap and atheroma[65]. Curiously, treatment of ApoE-/- mice with antibodies to collagen VI reduced atherosclerosis but its exact role has remained unknown[66]. We and others detected Collagen VI in sEVs but its functional significance remained unknown[23, 67]. Here we showed that collagen VI is essential for early FA formation at the VSMC periphery as well as VSMC invasion in a 3D model. We propose that collagen VI modulates FA formation either by activating cellular signalling or acting as a structural component changing local ECM stiffness[12]. Identified collagen VI receptors include α3β1 integrin, the cell surface proteoglycan chondroitin sulfate proteoglycan-4 (CSPG4; also known as NG2), and the anthrax toxin receptors 1 and 2[68-71]. Interestingly, a novel, recently identified Collagen VI signalling receptor (CMG2/ANTXR2) mediates localised Rho activation upon collagen VI binding[71, 72]. NG2 also activates the Rho/ROCK pathway leading to effective amoeboid invasiveness of tumour cells which is characterised by excessive blebbing and enhanced actomyosin contractility[60, 73]. Hence, biding of collagen VI to these receptors can potentially locally activate Rho and trigger FA formation and actomyosin contractility thus increasing VSMC motility and directional invasiveness. Of note, it was also reported that NG2 expression is elevated in VSMCs in the atherosclerotic plaque and NG2 knockout prevents plaque formation[45, 74]. Curiously, endotrophin, collagen VI α3 chain-derived profibrotic fragment has recently been associated with a higher risk of arterial stiffness and cardiovascular and all-cause death in patients with diabetes type 1 and atherosclerosis, respectively[75, 76]. Hence, targeting this novel sEV-dependent mechanism of VSMC invasion may open-up new therapeutic opportunities to modulate atherosclerotic plaque development or even to prevent undesired VSMC motility in restenosis.

We also identified a positive feedback loop and showed that FN stimulates sEV secretion by VSMCs. sEV secretion is a tightly regulated process which is governed by activation of signalling pathways including activation of G-protein coupled receptors[31] and alterations in cytosolic calcium[77], small GTPases Rab7, Rab27a, Rab27b and Rab35[78, 79], vesicular trafficking scaffold proteins including syntenin[80], sortillin[81] and CD63[82] or accumulation of ceramide[26]. We found that the fibrillar ECM proteins, FN and collagen I induce sEV secretion by activating the β1 integrin/FAK/Src and Arp2/3-dependent pathways. Our *in vivo* FN staining data are in good agreement with previous studies showing accumulation of FN in late-stage plaques[6, 7]. Moreover, we observed close co-distribution of FN and CD81 in the plaque suggesting that accumulating FN matrices can stimulate sEV secretion *in vivo*. Notably, expression of the major FN receptor, α5β1 integrin is re-activated upon VSMC de-differentiation following vascular injury[83]. It is thought the α5β1 integrin mediates FN matrix assembly, whilst β3 integrins are important for cell-matrix interactions[83, 84]. Our data sheds new light on the functional role of α5β1 as an ECM sensor inducing production of collagen VI-loaded sEVs which in turn enhance cell invasion in the complex ECM meshwork. Excessive collagen and elastin matrix breakdown in atheroma has been tightly linked to acute coronary events hence it will be interesting to study the possible link between sEV secretion and plaque stability as sEV-dependent invasion is also likely to influence the necessary ECM degradation induced by invading cells [85].

In summary, cooperative activation of integrin signalling and F-actin cytoskeleton pathways results in strict spatiotemporal control of the secretion of sEVs controlling cell-ECM crosstalk. Further studies are needed to test these mechanisms across various cell types and ECM matrices.

Materials and Methods

Materials

Proteins were fibronectin (Cell Guidance Systems, AP-23), collagen I (Gibco, #A1048301), laminin (Roche, 11243217001), Matrigel (Corning, #356237), Phalloidin-rhodamin (ThermoFisherScientific, R415). Peptides were Gly-Arg-Gly-Asp-Ser-Pro (GRGDSP, Merck, SCP0157) and scramble control Gly-Arg-Ala-Asp-Ser-Pro (GRADSP, Merck, SCP0156). All chemical inhibitors were diluted in DMSO and were: 3-O-Methyl-Sphingomyelin (SMPD3 inhibitor, Enzo Life technologies, BML-SL225-0005), FAM14 inhibitor (FAK inhibitor, Abcam, ab146739), PP2 (Src inhibitor, Life technologies, PHZ1223), CK666 (Arp2/3 inhibitor, Abcam ab141231), SMIFH2 (Formin inhibitor, Sigma, S4826). Control siRNA pool (ON-TARGETplus siRNA, Dharmacon, D-001810-10-05), collagen VI siRNA ON-TARGETplus siRNA (*COL6A3*, Human), SMARTPool, Horizon, L-003646-00-0005). Antibodies were CD9 (SA35-08 clone, NBP2-67310, Novus Biologicals), CD63 (BD Pharmingen, 556019), CD81 (BD Pharmingen™, 555676, B-11, SantaCruz, sc-166029 and M38 clone, NBP1-44861, Novus Biologicals), Syntenin-1 (Abcam, ab133267), Syndecan-4 (Abcam, ab24511), α-Actinin-4 (Abcam, ab108198), fibronectin (Abcam, ab2413, ab6328 [IST-9] (3D matrix staining) and F14 clone, ab45688 (clinical samples analysis)), β1 activating (12G10) antibody was previously described[86], 4B4 integrin inhibiting antibody (Beckman Coulter, 41116015), vinculin (Sigma, V9264), α5 integrin (P1D6, Abcam, ab78614), Myo10 (Sigma, HPA024223), gelatin-3BP/MAC-2BP (R&D systems, AF2226), EDIL3 antibody (R&D systems, MAB6046), TGFBI (Sigma, SAB2501486), IgG mouse (Sigma PP54), Anti-collagen Type VI antibody, clone 3C4 (Sigma, MAB1944), p34-Arc/ARPC2 antibody (Millipore, #07-227), Cortactin, LGALS3BP (R&D, AF2226), GAPDH (ab139416, Abcam). DNA plasmids were: CD63-GFP was kindly provided by Dr Aviva Tolkovsky[87], CD63-pHluorin was previously described[31], CD63-RFP was previously published[88], Paxillin-RFP was previously described[86], ARPC2–GFP DNA vector was kind gift from Professor Michael Way laboratory[34], F-tractin-RFP was kindly provided by Dr Thomas S. Randall (King's College London, UK), Myo10-GFP (Addgene Plasmid#135403) was previously described[89].

Cell culture

Human VSMCs were isolated as previously described[90] and were cultured in Dulbecco's modified Eagle medium (Sigma) supplemented with 20% fetal calf serum, 100 U/ml penicillin, 100 µg/ml streptomycin and 2 mmol/L L-glutamine (Gibco) and used between passages 4 and 12.

VSMC adhesion

24 well plate (Corning Costar) was incubated with 5µg/ml fibronectin in PBS overnight at +4°C. Next, sEVs (10µg/ml) diluted in PBS were added to the wells and incubated overnight at +4°C. Wells were washed with PBS, blocked with PBS-1% BSA for 30min at 37°C and washed 3 times with PBS again. VSMCs were incubated in serum free media, M199 supplemented with 0.5% BSA, 100 U/ml penicillin and 100µg/ml streptomycin overnight and removed by brief trypsin treatment. Next, 20,000 cells were added to each well and incubated for 30min at +37°C. Unattached cells were washed away with PBS and attached cells were fixed with 3.7% PFA for 15 min at 37°C. Cells were washed with H_2O 3 times and stained with 0.1% crystal violet for 30min at 10% CH_3COOH for 5min at room temperature. Samples were transferred to 96 well plate and absorbance was measured at 570nm using the spectrophotometer (Tecan GENios Pro).

iCELLigence adhesion protocol

E-Plate L8 (Acea) was coated with FN (5µg/mL) in PBS at 4°C overnight. Next, E-Plate L8 was gently washed once with cold PBS followed by the incubation with EV or sEV (10µg/ml) at 4°C overnight.

The following day, E-Plate L8 was incubated with 0.1% BSA in PBS for 30min at 37°C to block non-specific binding sites and washed with PBS before adding 250µL of M199 media supplemented with 20% exosome-free FBS. VSMCs were serum-deprived by incubation in M199 media supplemented with 0.5% BSA overnight, were passaged with trypsin and resuspended in media M199 supplemented with 20% exosome-free FBS to a final concentration 80,000 cells/mL. Cell aliquot (250µL) was added to E8-plate L8 which was then transferred to iCELLigence device for the adhesion assay. Cell adhesion was measured at 37°C with time intervals 20sec for 1h.

Focal adhesion turnover assay

iBIDI 35mm dishes were incubated with FN (5µg/ml) in PBS overnight at +4◦C and treated with exosomes (10µg/ml) diluted in PBS overnight at +4◦C. 500,000 cells were transfected with Paxillin-RFP/Myo10-GFP by using electroporation (see below) and plated on iBIDI 35mm dishes coated with FN and sEVs in DMEM supplemented with 20% exosome-free FBS, 100 U/ml penicillin, and 100 µg/ml streptomycin. Next, cells were transferred to DMEM supplemented with 20% exosome-free FBS, 10mM HEPES, 100 U/ml penicillin, and 100 µg/ml streptomycin and images were acquired (Nikon Spinning Disk) every 1min for 30min at 37°C. FA images were extracted from timelapses and FA turnover was quantified using Mathematica by producing the adhesion map as previously described[39].

Confocal spinning disk microscopy and live cell imaging

VSMC were transfected using electroporation (see below) and plated onto FN-coated 35mm iBIDI glass bottom dish and incubated for 48h. Then cells were transferred to DMEM supplemented with 20% exosome-free FBS, 10mM HEPES, 100 U/ml penicillin, and 100 µg/ml streptomycin and images were acquired every 1min for 20min at 37°C using a Nikon Ti-E (inverted) microscope equipped with a Yokogawa spinning disk and a Neo 5.5 sCMOS camera (Andor) and 60x or 100x/1.40 NA Plan Apo λ oil objectives (Nikon) were used. Images were acquired using NIS Elements AR 4.2 software. Cells were maintained at 37°C, 5% CO_2 throughout the experiment via a CO_2 chamber and a temperature-regulated Perspex box which housed the microscope stage and turret.

iSIM

Slides was imaged and super-resolved images collected using a Visitech-iSIM module coupled to a Nikon Ti-E microscope using a Nikon 100x 1.49NA TIRF oil immersion lens. Blue fluorescence was excited with a 405nm laser and emission filtered through a 460/50 filter. Green fluorescence was excited with a 488nm laser and emission filtered through a 525/50 filter. Red Fluorescence was excited with a 561nm laser and emission filtered through a 630/30 filter. Far Red fluorescence was excited with a 640nm laser and emission filtered through a 710/60 filter. Images were collected at focal planes spaced apart by 0.08um. Data was deconvolved using a Richardson-Lucy algorithm utilizing 20 iterations using the Nikon deconvolution software module (Nikon Elements). 65 stack images were taken with Z step 0.08µm. ImageJ (153t) or NIS Elements (5.21.00, built1483, 64bit) software were used for image analysis and assembly.

Cell electroporation

iBidi dishes were coated with FN (5µg/ml) in PBS for 1 hour at 37°C or overnight at 4°C. VSMCs were grown to 70% confluence, washed twice with EBSS and detached by trypsin treatment for 5min at +37°C. Cells (500,000) were mixed with plasmids (2.5µg each) in electroporation buffer (100µl, Lonza) and transfected using either Nucleofector II (program U25) or Nuclefector III (program CM-137).

Isolation of apoptotic bodies, extracellular vesicles and small extracellular vesicles

Flasks (T150) were incubated with PBS or FN (5µg/ml) in PBS overnight at +4°C and VSMCs (≈10^6 cells) were plated and incubated for 16h at +37°C. Next, cells were washed with EBSS 3 times and incubated with DMEM supplemented with 0,1% BSA, 100 U/ml penicillin, and 100 µg/ml streptomycin. Conditioned media was collected and centrifuged at 2,500 rpm (Thermo Scientific Heraeus Multifuge 3SR+ centrifuge, rotor Sorvall 75006445) for 5min to remove apoptotic bodies (AB, 1.2K pellet). Supernatant was transferred to centrifugation tube (Nalgene™ Oak Ridge High-Speed Polycarbonate Centrifuge Tubes, Thermo Fisher Scientific, 3138-0050) and centrifuged 10,000 x*g* for 30min. 10K pellet (EVs) was collected, washed in PBS once and kept at -80°C until further analysis. 10K supernatant was transferred to ultracentrifugation tubes (Polycarbonate tubes for ultracentrifugation, BeckmanCoulter, 355647) and centrifuged at 35,000 rpm (100,000x*g*) for 40min at 4°C (Fixed-angle rotor, Beckman Coulter Optima Max Unltracentrifuge). 100K pellet (sEVs) was washed with PBS twice and re-suspended in PBS. EV and sEV pellets were kept at -80°C for the proteomic analysis and freshly isolated sEVs were used for all other assays.

EV and sEV proteomic analysis

EV and sEV samples were submitted to the CEMS Proteomics Facility in the James Black Centre, King's College London for mass spectrometric analysis. The data were processed by Proteome Discover software for protein identification and quantification. Scaffold 5 proteome software was utilized to visualize differential protein expression. Individual proteins intensities were acquired and transformed to log2 scale before Hierarchical clustering analysis based on Euclidean distance and k-means processing. Differential genes defined by multiple groups comparation were applied to perform the gene ontology functional assay through using the DAVID Gene Ontology website (https://david.ncifcrf.gov/). Selected genes which showed abundant in each condition were applied to generate Venn diagram through Interacti website (http://www.interactivenn.net/).

Cell lysis

Cells were washed with PBS and removed by cell-scraper in 1ml of PBS. The cells were pelleted by centrifugation at 1000x*g* for 5min and cell pellets were kept at -80°C until further analysis. To prepare cell lysates, pellets were incubated with lysis buffer (0.1M TrisHCl(pH8.1), 150 mM NaCl, 1% Triton X-100 and protease inhibitors cocktail (Sigma, 1:100)) for 15min on ice. Cell lysates were subjected to ultrasound (Branson Sonifier 150), centrifuged at 16,363x*g* for 15 minutes (Eppendorf) at 4˚C and supernatants were collected and analysed by western blotting.

CD63-bead capturing assay

CD63-bead capturing assay was conducted as previously described[23] with some modifications. In brief, CD63 antibody (35µg) was immobilised on 1x10^8 4µm aldehyde-sulfate beads (Invitrogen) in 30mM MES buffer (pH 6.0) overnight at room temperature and spun down by centrifugation (3,000x*g*, 5min). Next, beads were washed 3 times with PBS containing 4%BSA and kept in PBS containing 0,1% Glycine and 0,1% NaN_3 at +4°C. VSMCs were plated onto 24 well plate (10,000 cells per well) and incubated in the complete media overnight. Next, cells were washed 3 times with EBSS and incubated in M199 supplemented with 2.5% exosome-free FBS in the presence of absence of inhibitors for 2h. Then, conditioned media was replaced once to the fresh aliquot of 2.5% exosome-free FBS in the presence or absence of inhibitors and cells were incubated for 18-24h. VSMC conditioned media was collected and centrifuged and centrifuged at 2,500x*g* for 5 min. VSMCs were detached from the plate by trypsin treatment and viable cells were quantified using NC3000 (ChemoMetec A/S). The conditioned media supernatants were mixed with 1µL of anti-CD63-coated

beads and incubated on a shaker overnight at +4°C. Beads were washed with PBS-2%BSA and incubated with anti-CD81-PE antibody (1:50 in PBS containing 2% BSA) for 1h at room temperature. Next, beads were washed with PBS-2%BSA and PBS and analysed by flow cytometry (BD Accuri™ C6). sEV secretion (fold change) was calculated as ratio of Arbitrary Units (fluorescence units x percentage of positive beads and normalized to the number of viable VSMCs) in the treatment and control conditions.

Exosome labelling with Alexa Fluor® 568 C5 Maleimide

Exosomes (10µg/ml) were incubated with 200µg/mL Alexa Fluor® 568 C5 Maleimide (ThermoFisherScientific, #A20341) in PBS for 1h at room temperature. An excessive dye was removed by using Exosome Spin Columns (MW 3000, ThermoFisherScientific, #4484449) according to the manufacturer protocol.

Fetuin-A and Fibronectin labelling and uptake studies.

Bovine fetuin-A (Sigma) and Fibronectin were labelled using an Alexa488 (A10235) and Alex568 (A10238) labelling kits in accordance with the manufacturer's protocol (Invitrogen). VSMCs were serum-starved for 16h and then incubated with Alexa488-labeled fetuin-A (10µg/mL) and Alexa555-labeled fibronectin (10µg/mL) from 30 to 180 minutes at 37°C.

VSMC and beads-coupled sEVs flow cytometry.

VSMC were removed from the plate by brief trypsin treatment, washed with M199 media supplemented with 20% FBS and resuspended in HBSS supplemented with 5%FBS. Cells were kept on ice throughout the protocol. Next, cells (200,000) were incubated with primary antibody for 30min on ice, washed with HBSS-5%FBS and incubated with secondary fluorescently-labelled antibody 30min on ice. Then cells were washed twice with HBSS-5%FBS and once with PBS and analysed by flow cytometry (BD FACScalibur, BD Bioscience).

Flow cytometry analysis of beads-coupled sEVs was conducted as described before[91]. In brief, exosomes (10µg) isolated by differential centrifugation were coupled to 4µm surfactant-free aldehyde/sulfate latex beads (Invitrogen) and were incubated with primary antibody and fluorescently labeled secondary antibody and analysed by flow cytometry on BD FACScalibur (BD Bioscience). Data were analysed using the Cell Quest Software (BD). Cells and beads stained with isotype-control antibodies were used as a negative control in all experiments.

Nanoparticle Tracking Analysis

Exosomes were diluted 1:150 and analysed using LM-10 using the light scattering mode of the NanoSight LM10 with sCMOS camera (NanoSight Ltd, Amesbury, United Kingdom). 5 frames (30 s each) were captured for each sample with camera level 10 and background detection level 11. Captured video was analysed using NTA software (NTA 3.2 Dev Build 3.2.16).

Western blotting

For western blotting, cell lysates or apoptotic bodies, microvesicles and exosomes in Laemmli loading buffer were separated by 10% SDS-PAGE. Next, separated proteins were transferred to ECL immobilon-P membranes (Millipore) using semi-dry transfer (BioRad). Membranes were incubated in the blocking buffer (TBST supplemented with 5% milk and 0.05% tween-20) for 1h at room temperature, then incubated with primary antibody overnight at +4°C. Next, membranes were washed with blocking buffer and incubated with secondary HRP-conjugated antibody and washed again in PBS supplemented with 0.05% tween-20 and PBS. Protein bands were detected using ECL

plus (Pierce ECL Western Blotting Substrate, #32109). Alternately, membranes were incubated with the secondary fluorescent antibody (Alexa fluor antibody) and washed again with TBST or PBST. Blots were detected using Odyssey Licor.

Generation of 3D matrix

Generation of 3D matrices were conducted as previously described[24] with some modifications. In brief, plates or glass coverslides were covered with 0.2% gelatin in PBS for 1h at 37°C. Wells were washed with PBS and fixed with 1% glutaraldehyde in PBS for 30min at room temperature. Plates were washed with PBS and incubated with 1M ethanolamine for 30min at room temperature, then washed with PBS again. VSMCs (5×10^5 per well) were plated and cultured for 24h. Then the medium was replaced with medium containing 50µg/ml of ascorbic acid and cells were incubated for 9days. The medium was replaced every 48h. To extract matrix, cells were rinsed with PBS and incubated with pre-warmed extraction buffer (20mM NH_4OH containing 0.5%Triton X-100) for 3min until intact cells are not seen. Next, equal volume of PBS was added to extraction buffer and plates were incubated for 24h at +4°C. Plates were washed with PBS twice and kept with PBS containing 100 U/ml penicillin and 100 µg/ml streptomycin up to 2 weeks at +4°C.

Immunocytochemistry

VSMCs (10,000 cells per well) were plated onto the coverslips and incubated for 48h. Next, cells were treated with inhibitors in M199 supplemented with 2.5% exosome-free FBS and fixed using 3.7% paraformaldehyde for 15 minutes at +37°C. Cells were then washed with PBS, permeabilised with PBS-0,1% triton X-100 for 5 min at room temperature and washed with PBS again. Cells were blocked with PBS-3% BSA for 1 hour at room temperature and incubated with primary antibodies overnight at +4°C. Following washing 3 times with PBS-3% BSA cells were incubated with secondary fluorescently-labelled antibodies in the dark for 1 hour at room temperature, stained with DAPI for 5min and mounted onto 75-Superdex slides using gelvatol mounting media and analysed by spinning disk confocal microscopy as above (Nikon). Primary antibodies were used in the following dilutions: CD63 1:500, Cortactin 1:500, Arp2C 1:500, Myo10 1:250, Vinculin 1:500, fibronectin 1:500, CD81 1:500, Rhodamine phalloidin 1:200 and secondary fluorescently labelled antibodies 1:200.

Focal adhesion turnover/Individual traction force

PDMS pillar (500 nm diameter, 1.3 µm height, 1µm centre-to-centre) substrates were prepared as described previously[92]. Briefly, Cd$Eq3: T_{tilt}(\nu) = a\frac{(1+\nu)}{2\pi}\left\{2(1-\nu) + \left(1 - \frac{1}{4(1-\nu)}\right)\right\}$SeS/ZnS alloyed quantum dots (490nm, Sigma) were spun on the master 30s at 10,000rpm with a 150i spin processor (SPS), before the addition of PDMS. PDMS (Sylgard 184, Dow Corning) was mixed thoroughly with its curing agent (10:1), degassed, poured over the silicon master, placed upside-down on a plasma-treated coverslip-dish (Mattek), or coverslip 4-well dishes (Ibidi) and cured at 80C for 2h. The mold was then removed and the pillars were incubated with fibronectin for 1h at 37C, after which pillars were incubated with sEVs (10µg/ml in PBS) at 4°C overnight.
VSMC previously transfected with Paxillin-RFP by using electroporation as above were plated on the Pillars and imaged on a Nikon Eclipse Ti-E epifluorescent microscope with a 100x 1.4NA objective, Nikon DS-Qi2 Camera and a Solent Scientific chamber with temperature and CO_2 control. For calculation of pillar displacements, a perfect grid was assumed and deviations from the grid were calculated using reference pillars outside the cell. The traction stress was calculated for a 10 µm wide region at the cell edge that was enriched in paxillin staining, taking into account all pillar displacements above a ~20 nm noise level, which was calculated from pillars outside the cells.

The Stiffness of the pillars was calculated as described by Ghibaudo et al[44] but taking into account substrate warping as described by Schoen et al (Eq1-5)[43]:

$$Eq1:\ k_{bend} = \frac{3}{64}\pi E \frac{D^4}{H^3};$$

$$Eq2: corr = \frac{\frac{16}{3}(\frac{L}{D})^3}{(\frac{16}{3}(\frac{L}{D})^3 + \frac{7+6\nu}{3}\frac{L}{D} + 8T_{tilt}(\nu)(\frac{L}{D})^2)};$$

$$Eq3: T_{tilt}(\nu) = a\frac{(1+\nu)}{2\pi}\left\{2(1-\nu) + \left(1 - \frac{1}{4(1-\nu)}\right)\right\}$$

$$Eq4: k = k_{bend} * corr;$$

$$Eq5: E_{Eff} = \frac{9k}{4\pi a};$$

Protein concentration

Protein concentration was determined by DC protein assay (BioRad).

Focal adhesion TIRF Imaging

µ-Slides (iBidi) were coated with FN (5µg/mL) in PBS at 4°C overnight. Next, µ-Slides were gently washed once with cold PBS following incubation with EV or sEV at 4°C overnight. The following day µ-Slides were incubated with 0.1% BSA in PBS for 30 minutes at 37°C to block non-specific binding sites and washed with PBS three times and 250µL of M199 media supplemented with 20% sEV-free FBS was added to each well. VSMCs were incubated in M199 media supplemented with 0.5% BSA overnight, detached with trypsin and resuspended to 80,000 cells/mL in M199 supplemented with 20% FBS. Cells (250µL) were added to µ-Slides and were incubated for 30min at 37°C. VSMC were fixed with 4% PFA for 10 minutes at 37°C, washed with PBS three times and were permeabilised with PBS supplemented with 0.2% Triton X-100 for 10 minutes at 37°C. Next, VSMC were washed three times with PBS for 5 minutes and were incubated with 3% BSA in PBS for 1h at room temperature. VSMC were incubated with anti-vinculin antibody (1:400) in blocking buffer at 4°C overnight. Next, VSMC were washed with PBS for 5min and incubated with secondary antibody (1:500, AlexaFluor488) diluted in blocking buffer for 1h at room temperature. Cells were incubated with CellMaskRed (ThermoFisherScientific) and DAPI (0.1 mg/mL) for 5min, washed and analysed by TIRF microscopy.

TIRF Microscopic images were collected on a Nikon Ti2 upright microscope with a TIRF illuminator (Nikon) attached using a 100x oil immersion (1.49 NA) objective lens. In each fluorescent channel the sample was excited with a laser beam at an angle indicated as follows (488nm at 62.3°, 561nm at 62.5° and 640nm at 65.5°). All emission light was filtered through a quad channel filter set (Chroma 89000) in the upper filter turret and a secondary bandpass emission filter in the lower turret position was used as follows for each channel (488nm excited: filter BP 525/50 - Chroma; 561nm excited: filter BP 595/50 - Chroma; 640nm excited: filter BP 700/75 - Chroma). Light was then passed to a Hamamatsu Orca-Flash 4v3.0 sCMOS camera and exposures for channels was set as follows (488nm: 100ms, 561nm: 100ms, 640nm:50ms) with 16bit channel images collected.

Acquisition was all controlled through NIS-Elements software (Nikon). Analysis of TIRF images was completed using NIS-Elements General Analysis Module. A general description of the process follows: Cell Area measurements were determined by use of an intensity threshold on the HCS CellMask Deep Red channel at an intensity of 100 AU (grey levels or arbitrary units) above the background to mask

the cell. The Cell area, whole cell Vinculin and Far-Red intensity measurements calculated from this binary region. In addition, an inversion of the cell mask binary was generated to have a means to measure distance to edge of the cell.

Vinculin derived Foci were masked using an intensity-based threshold (Above 10000 AU) and a size minimum for objects was set to 0.5µm^2 to eliminate smaller non foci objects from the binary mask. The foci mask was then limited to the cell mask regions to allow interpretation of the foci in the cell area. Minimum Distance to the outside of the cell for each foci was calculated by measurement of the nearest distance to the inverted non-cell mask. The average distance was then recorded for each image. For each foci intensity measurements were taken for the Vinculin and FarRed channel and the Mean intensity of the foci were recorded.

2D VSMC migration time lapse assay

24 well plates were incubated with FN (5µg/ml) in PBS overnight at +4°C and treated with sEVs (10µg/ml) diluted in PBS overnight at +4°C. VSMC (8,000 cells per well) were plated on the plate in M199 supplemented with 20% exosome-free FBS and incubated for 16h. Cells were washed twice with DMEM supplemented with 2.5% exosome-free FBS and incubated in this media for 2hrs +/- 3'-OMS. Media was replaced for a fresh aliquot and cells were imaged using Opera Phenix High Content Screening System (PerkinElmer) every 6min20sec for 8h in a transmitted light channel. Quantification of cellular velocity and directionality was performed in Harmony 4.9 (Perkin Elmer).

3D VSMC Invasion time lapse assay

Acquisition. Migration assay were completed using IBidi Chemotaxis µ-slides (Ibidi µ-slides #80326). VSMC were deprived overnight in M199 supplemented with 0.5% BSA, counted and mixed with Matrigel supplemented with/without sEV (5ug total in 100µl volume) to a final cell concentration of ca. 3 x 10^6 cells/ml and stained with Draq5 according to the manufacturer protocol. Slides were left for 30min at 37°C for gelation and chemoattractant-free medium (65uL of M199 supplemented with 0.5% BSA) was filled through Filling Port E. Next, the empty reservoir was filled by injecting chemoattractant medium (65uL of M199 supplemented with 20% FBS exosome-free through Filling Port C. 3 slides were loaded and cells were imaged with the Opera Phenix (Perkin Elmer) high content imaging platform (10x Objective NA 0.3). Images were collected for digital phase contrast and a fluorescence channel for Draq5. Fluorescence was obtained by exciting with a 640nm laser and emission light was filtered with a 700/75 bandpass filter to a sCMOS camera. Images were recorded every 10min for 12h in several locations for each slide.

Migration tracking and analysis of tracking. Analysis of cell motion was completed on Draq5 images using Harmony Software (Perkin Elmer) with measurements of cell area, speed and direction were obtained for each cell/track and timepoint. Cells were not selected for tracking if they were in proximity to other cells of a distance of 35µm. The measurements and object data were exported and further analysis was performed. Data for each track included total length (timepoints), speed(µm/s), Straightness, accumulated distance (µm), lateral displacement (µm) and vertical displacement (µm).

Data analysis. This data was then analysed using an in-house script using Python library Pandas. Tracks were discarded if they were less than 3 time-points in length. Means and Standard Deviations were calculated for track length (timepoints), Speed (µm/s), Track Straightness and accumulated distance. For each track the Parallel FMI (forward motion index) was calculated by taking a ratio of vertical displacement to accumulated distance. The means and standard deviations for these were calculated and reported for each condition similarly. Track Straightness is calculated as the ratio of total

displacement over total track length. Accumulated distance is the total length of the track from the first to last time point of the track.

Clinical samples

Patients enrollment. The study was approved by the Local Ethical committee of the Research Institute for Complex Issues of Cardiovascular Diseases (Kemerovo, Russia, protocol number 20200212, dates of approval: 12 February 2020), and a written informed consent was provided by all study participants after receiving a full explanation of the study. The investigation was carried out in accordance with the Good Clinical Practice and the Declaration of Helsinki. Criteria of inclusion were: 1) performance of carotid endarterectomy due to chronic brain ischemia or ischemic stroke; 2) a signed written informed consent to be enrolled. A criterion of exclusion was incomplete investigation regardless of the reason; in this case, we enrolled another subject with similar age, gender and clinicopathological features who met the inclusion criteria. Cerebrovascular disease (chronic brain ischemia and ischemic stroke) as well as comorbid conditions (arterial hypertension, chronic heart failure, chronic obstructive pulmonary disease, asthma, chronic kidney disease, diabetes mellitus, overweight and obesity) were diagnosed and treated according to the respective guidelines of European Society of Cardiology, Global Initiative for Chronic Obstructive Lung Disease, Global Initiative for Asthma, Kidney Disease: Improving Global Outcomes, American Diabetes Association, and European Association for the Study of Obesity. eGFR was calculated according to the Chronic Kidney Disease Epidemiology Collaboration (CKD-EPI) equation. Extracranial artery stenosis was assessed using the color duplex screening (Vivid 7 Dimension Ultrasound System, General Electric Healthcare). Data on age, gender, smoking status and pharmacological anamnesis were collected at the time of admission. In total, we enrolled 20 patients. The detailed characteristics of the study samples are presented in Table S1.

Sample collection and preparation. Carotid atherosclerotic plaques (n = 14) and adjacent intact arterial segments (n = 14) were pairwise excised during the carotid endarterectomy and divided into 3 segments each. The first segment was snap-frozen in the optimal cutting temperature compound (Tissue-Tek, 4583, Sakura) using a liquid nitrogen and was then sectioned on a cryostat (Microm HM525, 387779, Thermo Scientific). To ensure the proper immunofluorescence examination, we prepared 8 sections (7µm thickness), evenly distributed across the entire carotid artery segment, per slide. The second and third segments were homogenised in TRIzol Reagent (15596018, Thermo Fisher Scientific) for RNA extraction or in T-PER Tissue Protein Extraction Reagent (78510, Thermo Fisher Scientific) supplied with Halt protease and phosphatase inhibitor cocktail (78444, Thermo Fisher Scientific) for the total protein extraction according to the manufacturer's protocols. Quantification and quality control of the isolated RNA was performed employing Qubit 4 fluorometer (Q33238, Thermo Fisher Scientific), Qubit RNA BR assay kit (Q10210, Thermo Fisher Scientific), Qubit RNA IQ assay kit (Q33222, Thermo Fisher Scientific), Qubit RNA IQ standards for calibration (Q33235, Thermo Fisher Scientific) and Qubit assay tubes (Q32856, Thermo Fisher Scientific) according to the manufacturer's protocols. Quantification of total protein was conducted using BCA Protein Assay Kit (23227, Thermo Fisher Scientific) and Multiskan Sky microplate spectrophotometer (51119700DP, Thermo Fisher Scientific) in accordance with the manufacturer's protocol.

Immunofluorescence examination. Upon the sectioning, vascular tissues were dried at room temperature for 30min, fixed and permeabilised in ice-cold acetone for 10min, incubated in 1% bovine serum albumin (Cat. No. A2153, Sigma-Aldrich) for 1h to block non-specific protein binding, stained with unconjugated mouse anti-human CD81 (M38 clone, NBP1-44861, 1:100, Novus Biologicals) and rabbit anti-human fibronectin (F14 clone, ab45688, 1:250, Abcam) primary antibodies and incubated

at 4°C for 16h. Sections were further treated with pre-adsorbed donkey anti-mouse Alexa Fluor 488-conjugated (ab150109, 1:500, Abcam) and donkey anti-rabbit Alexa Fluor 555-conjugated secondary antibodies (ab150062, 1:500, Abcam) and incubated for 1h at room temperature. Between all steps, washing was performed thrice with PBS (pH 7.4, P4417, Sigma-Aldrich). Nuclei were counterstained with 4′,6-diamidino-2-phenylindole (DAPI) for 30min at room temperature (10µg/mL, D9542, Sigma-Aldrich). Coverslips were mounted with ProLong Gold Antifade (P36934, Thermo Fisher Scientific). Sections were examined by confocal laser scanning microscopy (LSM 700, Carl Zeiss). Colocalization analysis (n=12 images) was performed using the respective ImageJ (National Institutes of Health) plugins (Colocalisation Threshold and Coloc2). To evaluate the colocalization, we calculated Pearson's r above threshold (zero-zero pixels), thresholded Mander's split colocalisation coefficient (the proportion of signal in each channel that colocalizes with the other channel) for both (red and green) channels, percent volume colocalised with each channel, and intensity volume above threshold colocalised with each channel in both neointima and media.

Reverse transcription-quantitative polymerase chain reaction (RT-qPCR). Reverse transcription was carried out utilising High Capacity cDNA Reverse Transcription Kit (4368814, Thermo Fisher Scientific). Gene expression was measured by RT-qPCR using the customised primers (500nmol/L each, Evrogen, Moscow, Russian Federation, Table S5), cDNA (20ng) and PowerUp SYBR Green Master Mix (A25778, Thermo Fisher Scientific) according to the manufacturer's protocol for Tm ≥ 60°C (fast cycling mode). Technical replicates (n=3 per each sample collected from one vascular segment) were performed in all RT-qPCR experiments. The reaction was considered successful if its efficiency was 90-105% and R^2 was ≥ 0.98. Quantification of the *CD9*, *CD63*, *CD81*, *COL6A3*, *EDIL3*, *CSPG4*, *TGFBI*, *FN1*, and *MYADM* mRNA levels in carotid atherosclerotic plaques (n=5) and adjacent intact arterial segments (n = 5) was performed by using the $2^{-\Delta\Delta Ct}$ method. Relative transcript levels were expressed as a value relative to the average of 3 housekeeping genes (*ACTB*, *GAPDH*, *B2M*).

Western blotting. Equal amounts of protein lysate (15µg per sample) of carotid atherosclerotic plaques (n=12), adjacent intact arterial segments (n=12), and plaque-derived sEVs (n=6) were mixed with NuPAGE lithium dodecyl sulfate sample buffer (NP0007, Thermo Fisher Scientific) at a 4:1 ratio and NuPAGE sample reducing agent (NP0009, Thermo Fisher Scientific) at a 10:1 ratio, denatured at 99°C for 5 minutes, and then loaded on a 1.5mm NuPAGE 4-12% Bis-Tris protein gel (NP0335BOX, Thermo Fisher Scientific). The 1:1 mixture of Novex Sharp pre-stained protein standard (LC5800, Thermo Fisher Scientific) and MagicMark XP Western protein standard (LC5602, Thermo Fisher Scientific) was loaded as a molecular weight marker. Proteins were separated by the sodium dodecyl sulphate-polyacrylamide gel electrophoresis (SDS-PAGE) at 150V for 2h using NuPAGE 2-(N-morpholino)ethanesulfonic acid SDS running buffer (NP0002, Thermo Fisher Scientific), NuPAGE Antioxidant (NP0005, Thermo Fisher Scientific), and XCell SureLock Mini-Cell vertical mini-protein gel electrophoresis system (EI0001, Thermo Fisher Scientific). Protein transfer was performed using polyvinylidene difluoride (PVDF) transfer stacks (IB24001, Thermo Fisher Scientific) and iBlot 2 Gel Transfer Device (IB21001, Thermo Fisher Scientific) according to the manufacturer's protocols using a standard transfer mode for 30-150 kDa proteins (P0 – 20 V for 1min, 23 V for 4min, and 25 V for 2 min). PVDF membranes were then incubated in iBind Flex Solution (SLF2020, Thermo Fisher Scientific) for 1h to prevent non-specific binding.

Blots were probed with rabbit primary antibodies to CD9, fibronectin or CD81, and GAPDH (loading control). Horseradish peroxidase-conjugated goat anti-rabbit (7074, Cell Signaling Technology) or goat anti-mouse (AP130P, Sigma-Aldrich) secondary antibodies were used at 1:200 and 1:1000 dilution, respectively. Incubation with the antibodies was performed using iBind Flex Solution Kit (SLF2020, Thermo Fisher Scientific), iBind Flex Cards (SLF2010, Thermo Fisher Scientific) and iBind Flex Western

Device (SLF2000, Thermo Fisher Scientific) during 3h according to the manufacturer's protocols. Chemiluminescent detection was performed using SuperSignal West Pico PLUS chemiluminescent substrate (34580, Thermo Fisher Scientific) and C-DiGit blot scanner (3600-00, LI-COR Biosciences) in a high-sensitivity mode (12min scanning). Densitometry was performed using the ImageJ software (National Institutes of Health) using the standard algorithm (consecutive selection and plotting of the lanes with the measurement of the peak area) and subsequent adjustment to the loading control (GAPDH).

Statistics

Data were analysed using GraphPad Prizm (version 8.4.3). CD63-beads assay, NanoView, adhesion assay, FA quantification and 2D migration multiple comparison data were analysed by one-way ANOVA test. Two group CD63-bead assay was analysed by non-paired T-test. VSMC invasion multiple comparison data were analysed using non-parametric Kruskal-Wallis test. Two group invasion data were analysed using non-parametric Kolmogorov-Smirnov test. Clinical data for two groups was analysed by non-paired T-test and multiple comparison was analysed by Mann-Whitney U-test. All analysis was conducted using PRISM software (GraphPad, San Diego, CA). Values of $P<0.05$ were considered statistically significant.

Short abbreviations

ECM extracellular matrix

EM electron microscopy

FN fibronectin

MVB multivesicular body

NTA nanoparticle tracking analysis

SMPD3 sphingomyelin phosphodiesterase 3

VSMC vascular smooth muscle cell

Acknowledgments

ANK and CS were supported by BHF-PG/17/37/33023. TI was supported by BHF PG/20/6/34835 and FS/14/30/30917. REC was supported by National Institutes of General Medical Sciences grant R01GM134531. AK, MS and LB were supported by the Ministry of Science and Higher Education of the Russian Federation-Complex Program of Basic Research under the Siberian Branch of the Russian Academy of Sciences within the Basic Research Topic of Research Institute for Complex Issues of Cardiovascular Diseases № 0419-2021-001.

Competing interests

A. Kapustin is currently an employee and shareholder of AstraZeneca.

References

1. Libby, P., Ridker, P.M. & Hansson, G.K. Progress and challenges in translating the biology of atherosclerosis. *Nature* **473**, 317-325 (2011).
2. Chappell, J. *et al.* Extensive Proliferation of a Subset of Differentiated, yet Plastic, Medial Vascular Smooth Muscle Cells Contributes to Neointimal Formation in Mouse Injury and Atherosclerosis Models. *Circ Res* **119**, 1313-1323 (2016).
3. Misra, A. *et al.* Integrin beta3 regulates clonality and fate of smooth muscle-derived atherosclerotic plaque cells. *Nat Commun* **9**, 2073 (2018).
4. Durham, A.L., Speer, M.Y., Scatena, M., Giachelli, C.M. & Shanahan, C.M. Role of smooth muscle cells in vascular calcification: implications in atherosclerosis and arterial stiffness. *Cardiovasc Res* **114**, 590-600 (2018).
5. Rohwedder, I. *et al.* Plasma fibronectin deficiency impedes atherosclerosis progression and fibrous cap formation. *EMBO Mol Med* **4**, 564-576 (2012).
6. Langley, S.R. *et al.* Extracellular matrix proteomics identifies molecular signature of symptomatic carotid plaques. *J Clin Invest* **127**, 1546-1560 (2017).
7. Glukhova, M.A. *et al.* Expression of extra domain A fibronectin sequence in vascular smooth muscle cells is phenotype dependent. *J Cell Biol* **109**, 357-366 (1989).
8. Pankov, R. & Yamada, K.M. Fibronectin at a glance. *J Cell Sci* **115**, 3861-3863 (2002).
9. Hocking, D.C., Sottile, J. & McKeown-Longo, P.J. Activation of distinct alpha5beta1-mediated signaling pathways by fibronectin's cell adhesion and matrix assembly domains. *J Cell Biol* **141**, 241-253 (1998).
10. Bass, M.D. *et al.* Syndecan-4-dependent Rac1 regulation determines directional migration in response to the extracellular matrix. *J Cell Biol* **177**, 527-538 (2007).
11. Nobes, C.D. & Hall, A. Rho, rac, and cdc42 GTPases regulate the assembly of multimolecular focal complexes associated with actin stress fibers, lamellipodia, and filopodia. *Cell* **81**, 53-62 (1995).
12. Sheetz, M.P., Felsenfeld, D.P. & Galbraith, C.G. Cell migration: regulation of force on extracellular-matrix-integrin complexes. *Trends Cell Biol* **8**, 51-54 (1998).
13. Ridley, A.J. Rho GTPases and cell migration. *J Cell Sci* **114**, 2713-2722 (2001).
14. Sung, B.H., Ketova, T., Hoshino, D., Zijlstra, A. & Weaver, A.M. Directional cell movement through tissues is controlled by exosome secretion. *Nat Commun* **6**, 7164 (2015).
15. Sung, B.H. & Weaver, A.M. Exosome secretion promotes chemotaxis of cancer cells. *Cell Adh Migr* **11**, 187-195 (2017).
16. Sung, B.H. *et al.* A live cell reporter of exosome secretion and uptake reveals pathfinding behavior of migrating cells. *Nat Commun* **11**, 2092 (2020).
17. Koumangoye, R.B., Sakwe, A.M., Goodwin, J.S., Patel, T. & Ochieng, J. Detachment of breast tumor cells induces rapid secretion of exosomes which subsequently mediate cellular adhesion and spreading. *PLoS One* **6**, e24234 (2011).
18. Hoshino, D. *et al.* Exosome secretion is enhanced by invadopodia and drives invasive behavior. *Cell Rep* **5**, 1159-1168 (2013).
19. Clayton, A. *et al.* Adhesion and signaling by B cell-derived exosomes: the role of integrins. *FASEB J* **18**, 977-979 (2004).
20. Brown, M. *et al.* Lymphatic exosomes promote dendritic cell migration along guidance cues. *J Cell Biol* **217**, 2205-2221 (2018).
21. Majumdar, R., Tavakoli Tameh, A. & Parent, C.A. Exosomes Mediate LTB4 Release during Neutrophil Chemotaxis. *PLoS Biol* **14**, e1002336 (2016).
22. Kriebel, P.W. *et al.* Extracellular vesicles direct migration by synthesizing and releasing chemotactic signals. *J Cell Biol* **217**, 2891-2910 (2018).
23. Kapustin, A.N. *et al.* Vascular smooth muscle cell calcification is mediated by regulated exosome secretion. *Circ Res* **116**, 1312-1323 (2015).

24. Beacham, D.A., Amatangelo, M.D. & Cukierman, E. Preparation of extracellular matrices produced by cultured and primary fibroblasts. *Curr Protoc Cell Biol* **Chapter 10**, Unit 10 19 (2007).
25. Kowal, J. *et al.* Proteomic comparison defines novel markers to characterize heterogeneous populations of extracellular vesicle subtypes. *Proc Natl Acad Sci U S A* **113**, E968-977 (2016).
26. Trajkovic, K. *et al.* Ceramide triggers budding of exosome vesicles into multivesicular endosomes. *Science* **319**, 1244-1247 (2008).
27. Klinghoffer, R.A., Sachsenmaier, C., Cooper, J.A. & Soriano, P. Src family kinases are required for integrin but not PDGFR signal transduction. *EMBO J* **18**, 2459-2471 (1999).
28. Jacquemet, G., Hamidi, H. & Ivaska, J. Filopodia in cell adhesion, 3D migration and cancer cell invasion. *Curr Opin Cell Biol* **36**, 23-31 (2015).
29. Svitkina, T.M. & Borisy, G.G. Arp2/3 complex and actin depolymerizing factor/cofilin in dendritic organization and treadmilling of actin filament array in lamellipodia. *J Cell Biol* **145**, 1009-1026 (1999).
30. Sinha, S. *et al.* Cortactin promotes exosome secretion by controlling branched actin dynamics. *J Cell Biol* **214**, 197-213 (2016).
31. Verweij, F.J. *et al.* Quantifying exosome secretion from single cells reveals a modulatory role for GPCR signaling. *J Cell Biol* **217**, 1129-1142 (2018).
32. Bohil, A.B., Robertson, B.W. & Cheney, R.E. Myosin-X is a molecular motor that functions in filopodia formation. *Proc Natl Acad Sci U S A* **103**, 12411-12416 (2006).
33. Heusermann, W. *et al.* Exosomes surf on filopodia to enter cells at endocytic hot spots, traffic within endosomes, and are targeted to the ER. *J Cell Biol* **213**, 173-184 (2016).
34. Abella, J.V. *et al.* Isoform diversity in the Arp2/3 complex determines actin filament dynamics. *Nat Cell Biol* **18**, 76-86 (2016).
35. Thomas, S., Popov, V.L. & Walker, D.H. Exit mechanisms of the intracellular bacterium Ehrlichia. *PLoS One* **5**, e15775 (2010).
36. Hutcheson, J.D. *et al.* Genesis and growth of extracellular-vesicle-derived microcalcification in atherosclerotic plaques. *Nat Mater* **15**, 335-343 (2016).
37. Tagliatela, A.C. *et al.* Coronin 1C inhibits melanoma metastasis through regulation of MT1-MMP-containing extracellular vesicle secretion. *Sci Rep* **10**, 11958 (2020).
38. Burridge, K. Foot in mouth: do focal adhesions disassemble by endocytosis? *Nat Cell Biol* **7**, 545-547 (2005).
39. Holt, M.R. *et al.* Quantifying cell-matrix adhesion dynamics in living cells using interference reflection microscopy. *J Microsc* **232**, 73-81 (2008).
40. Chrzanowska-Wodnicka, M. & Burridge, K. Rho-stimulated contractility drives the formation of stress fibers and focal adhesions. *J Cell Biol* **133**, 1403-1415 (1996).
41. Arthur, W.T. & Burridge, K. RhoA inactivation by p190RhoGAP regulates cell spreading and migration by promoting membrane protrusion and polarity. *Mol Biol Cell* **12**, 2711-2720 (2001).
42. Tabdanov, E. *et al.* Micropatterning of TCR and LFA-1 ligands reveals complementary effects on cytoskeleton mechanics in T cells. *Integr Biol (Camb)* **7**, 1272-1284 (2015).
43. Schoen, I., Hu, W., Klotzsch, E. & Vogel, V. Probing cellular traction forces by micropillar arrays: contribution of substrate warping to pillar deflection. *Nano Lett* **10**, 1823-1830 (2010).
44. Ghibaudo, M. *et al.* Traction forces and rigidity sensing regulate cell functions *Soft Matter* **4**, 1836-1843 (2008).
45. Tillet, E., Gential, B., Garrone, R. & Stallcup, W.B. NG2 proteoglycan mediates beta1 integrin-independent cell adhesion and spreading on collagen VI. *J Cell Biochem* **86**, 726-736 (2002).
46. Nishida, S. *et al.* Collagen VI suppresses fibronectin-induced enteric neural crest cell migration by downregulation of focal adhesion proteins. *Biochem Biophys Res Commun* **495**, 1461-1467 (2018).

47. Sardone, F. *et al.* Collagen VI-NG2 axis in human tendon fibroblasts under conditions mimicking injury response. *Matrix Biol* **55**, 90-105 (2016).
48. Pankova, K., Rosel, D., Novotny, M. & Brabek, J. The molecular mechanisms of transition between mesenchymal and amoeboid invasiveness in tumor cells. *Cell Mol Life Sci* **67**, 63-71 (2010).
49. Galbraith, C.G., Yamada, K.M. & Galbraith, J.A. Polymerizing actin fibers position integrins primed to probe for adhesion sites. *Science* **315**, 992-995 (2007).
50. Pollard, T.D. & Borisy, G.G. Cellular motility driven by assembly and disassembly of actin filaments. *Cell* **112**, 453-465 (2003).
51. Ridley, A.J. & Hall, A. The small GTP-binding protein rho regulates the assembly of focal adhesions and actin stress fibers in response to growth factors. *Cell* **70**, 389-399 (1992).
52. Price, L.S., Leng, J., Schwartz, M.A. & Bokoch, G.M. Activation of Rac and Cdc42 by integrins mediates cell spreading. *Mol Biol Cell* **9**, 1863-1871 (1998).
53. Ren, X.D., Kiosses, W.B. & Schwartz, M.A. Regulation of the small GTP-binding protein Rho by cell adhesion and the cytoskeleton. *EMBO J* **18**, 578-585 (1999).
54. Wang, H.R. *et al.* Regulation of cell polarity and protrusion formation by targeting RhoA for degradation. *Science* **302**, 1775-1779 (2003).
55. Rottner, K., Hall, A. & Small, J.V. Interplay between Rac and Rho in the control of substrate contact dynamics. *Curr Biol* **9**, 640-648 (1999).
56. Roberts, L.A., Glenn, H., Hahn, C.S. & Jacobson, B.S. Cdc42 and RhoA are differentially regulated during arachidonate-mediated HeLa cell adhesion. *J Cell Physiol* **196**, 196-205 (2003).
57. Nobes, C.D. & Hall, A. Rho GTPases control polarity, protrusion, and adhesion during cell movement. *J Cell Biol* **144**, 1235-1244 (1999).
58. Cox, E.A., Sastry, S.K. & Huttenlocher, A. Integrin-mediated adhesion regulates cell polarity and membrane protrusion through the Rho family of GTPases. *Mol Biol Cell* **12**, 265-277 (2001).
59. Matera, D.L., Lee, A.T., Hiraki, H.L. & Baker, B.M. The Role of Rho GTPases During Fibroblast Spreading, Migration, and Myofibroblast Differentiation in 3D Synthetic Fibrous Matrices. *Cell Mol Bioeng* **14**, 381-396 (2021).
60. Sahai, E. & Marshall, C.J. Differing modes of tumour cell invasion have distinct requirements for Rho/ROCK signalling and extracellular proteolysis. *Nat Cell Biol* **5**, 711-719 (2003).
61. Sanz-Moreno, V. *et al.* Rac activation and inactivation control plasticity of tumor cell movement. *Cell* **135**, 510-523 (2008).
62. Okada, M. *et al.* Primary collagen VI deficiency is the second most common congenital muscular dystrophy in Japan. *Neurology* **69**, 1035-1042 (2007).
63. Bryant, J.E. *et al.* Cardiac myofibroblast differentiation is attenuated by alpha(3) integrin blockade: potential role in post-MI remodeling. *J Mol Cell Cardiol* **46**, 186-192 (2009).
64. Luther, D.J. *et al.* Absence of type VI collagen paradoxically improves cardiac function, structure, and remodeling after myocardial infarction. *Circ Res* **110**, 851-856 (2012).
65. Katsuda, S. *et al.* Collagens in human atherosclerosis. Immunohistochemical analysis using collagen type-specific antibodies. *Arterioscler Thromb* **12**, 494-502 (1992).
66. Liu, X. *et al.* Collagen VI antibody reduces atherosclerosis by activating monocyte/macrophage polarization in ApoE(-/-) mice. *Int Immunopharmacol* **111**, 109100 (2022).
67. He, M. *et al.* Hepatocellular carcinoma-derived exosomes promote motility of immortalized hepatocyte through transfer of oncogenic proteins and RNAs. *Carcinogenesis* **36**, 1008-1018 (2015).
68. Doane, K.J., Howell, S.J. & Birk, D.E. Identification and functional characterization of two type VI collagen receptors, alpha 3 beta 1 integrin and NG2, during avian corneal stromal development. *Invest Ophthalmol Vis Sci* **39**, 263-275 (1998).

69. Nishiyama, A. & Stallcup, W.B. Expression of NG2 proteoglycan causes retention of type VI collagen on the cell surface. *Mol Biol Cell* **4**, 1097-1108 (1993).
70. Nanda, A. *et al.* TEM8 interacts with the cleaved C5 domain of collagen alpha 3(VI). *Cancer Res* **64**, 817-820 (2004).
71. Burgi, J. *et al.* CMG2/ANTXR2 regulates extracellular collagen VI which accumulates in hyaline fibromatosis syndrome. *Nat Commun* **8**, 15861 (2017).
72. Burgi, J. *et al.* Ligand Binding to the Collagen VI Receptor Triggers a Talin-to-RhoA Switch that Regulates Receptor Endocytosis. *Dev Cell* **53**, 418-430 e414 (2020).
73. Pankova, D. *et al.* NG2-mediated Rho activation promotes amoeboid invasiveness of cancer cells. *Eur J Cell Biol* **91**, 969-977 (2012).
74. She, Z.G. *et al.* NG2 Proteoglycan Ablation Reduces Foam Cell Formation and Atherogenesis via Decreased Low-Density Lipoprotein Retention by Synthetic Smooth Muscle Cells. *Arterioscler Thromb Vasc Biol* **36**, 49-59 (2016).
75. Holm Nielsen, S. *et al.* The novel collagen matrikine, endotrophin, is associated with mortality and cardiovascular events in patients with atherosclerosis. *J Intern Med* **290**, 179-189 (2021).
76. Frimodt-Moller, M. *et al.* A marker of type VI collagen formation (PRO-C6) is associated with higher arterial stiffness in type 1 diabetes. *Acta Diabetol* **56**, 711-712 (2019).
77. Savina, A., Furlan, M., Vidal, M. & Colombo, M.I. Exosome release is regulated by a calcium-dependent mechanism in K562 cells. *J Biol Chem* **278**, 20083-20090 (2003).
78. Jae, N., McEwan, D.G., Manavski, Y., Boon, R.A. & Dimmeler, S. Rab7a and Rab27b control secretion of endothelial microRNA through extracellular vesicles. *FEBS Lett* **589**, 3182-3188 (2015).
79. Savina, A., Vidal, M. & Colombo, M.I. The exosome pathway in K562 cells is regulated by Rab11. *J Cell Sci* **115**, 2505-2515 (2002).
80. Baietti, M.F. *et al.* Syndecan-syntenin-ALIX regulates the biogenesis of exosomes. *Nat Cell Biol* **14**, 677-685 (2012).
81. Goettsch, C. *et al.* Sortilin mediates vascular calcification via its recruitment into extracellular vesicles. *J Clin Invest* **126**, 1323-1336 (2016).
82. van Niel, G. *et al.* The tetraspanin CD63 regulates ESCRT-independent and -dependent endosomal sorting during melanogenesis. *Dev Cell* **21**, 708-721 (2011).
83. Pickering, J.G. *et al.* alpha5beta1 integrin expression and luminal edge fibronectin matrix assembly by smooth muscle cells after arterial injury. *Am J Pathol* **156**, 453-465 (2000).
84. Slepian, M.J., Massia, S.P., Dehdashti, B., Fritz, A. & Whitesell, L. Beta3-integrins rather than beta1-integrins dominate integrin-matrix interactions involved in postinjury smooth muscle cell migration. *Circulation* **97**, 1818-1827 (1998).
85. Libby, P. & Aikawa, M. Stabilization of atherosclerotic plaques: new mechanisms and clinical targets. *Nat Med* **8**, 1257-1262 (2002).
86. Parsons, M., Messent, A.J., Humphries, J.D., Deakin, N.O. & Humphries, M.J. Quantification of integrin receptor agonism by fluorescence lifetime imaging. *J Cell Sci* **121**, 265-271 (2008).
87. Bampton, E.T.W., Goemans, C.G., Niranjan, D., Mizushima, N. & Tolkovsky, A.M. The Dynamics of Autophagy Visualised in Live Cells: from Autophagosome Formation to Fusion with Endo/lysosomes. *Autophagy* **1**, 23-36 (2005).
88. Leifer, C.A. *et al.* TLR9 is localized in the endoplasmic reticulum prior to stimulation. *J Immunol* **173**, 1179-1183 (2004).
89. Berg, J.S. & Cheney, R.E. Myosin-X is an unconventional myosin that undergoes intrafilopodial motility. *Nat Cell Biol* **4**, 246-250 (2002).
90. Reynolds, J.L. *et al.* Human vascular smooth muscle cells undergo vesicle-mediated calcification in response to changes in extracellular calcium and phosphate concentrations: a potential mechanism for accelerated vascular calcification in ESRD. *J Am Soc Nephrol* **15**, 2857-2867 (2004).

91. Kapustin, A.N. *et al.* Calcium regulates key components of vascular smooth muscle cell-derived matrix vesicles to enhance mineralization. *Circ Res* **109**, e1-12 (2011).
92. Pandey, P. *et al.* Cardiomyocytes Sense Matrix Rigidity through a Combination of Muscle and Non-muscle Myosin Contractions. *Dev Cell* **45**, 661 (2018).

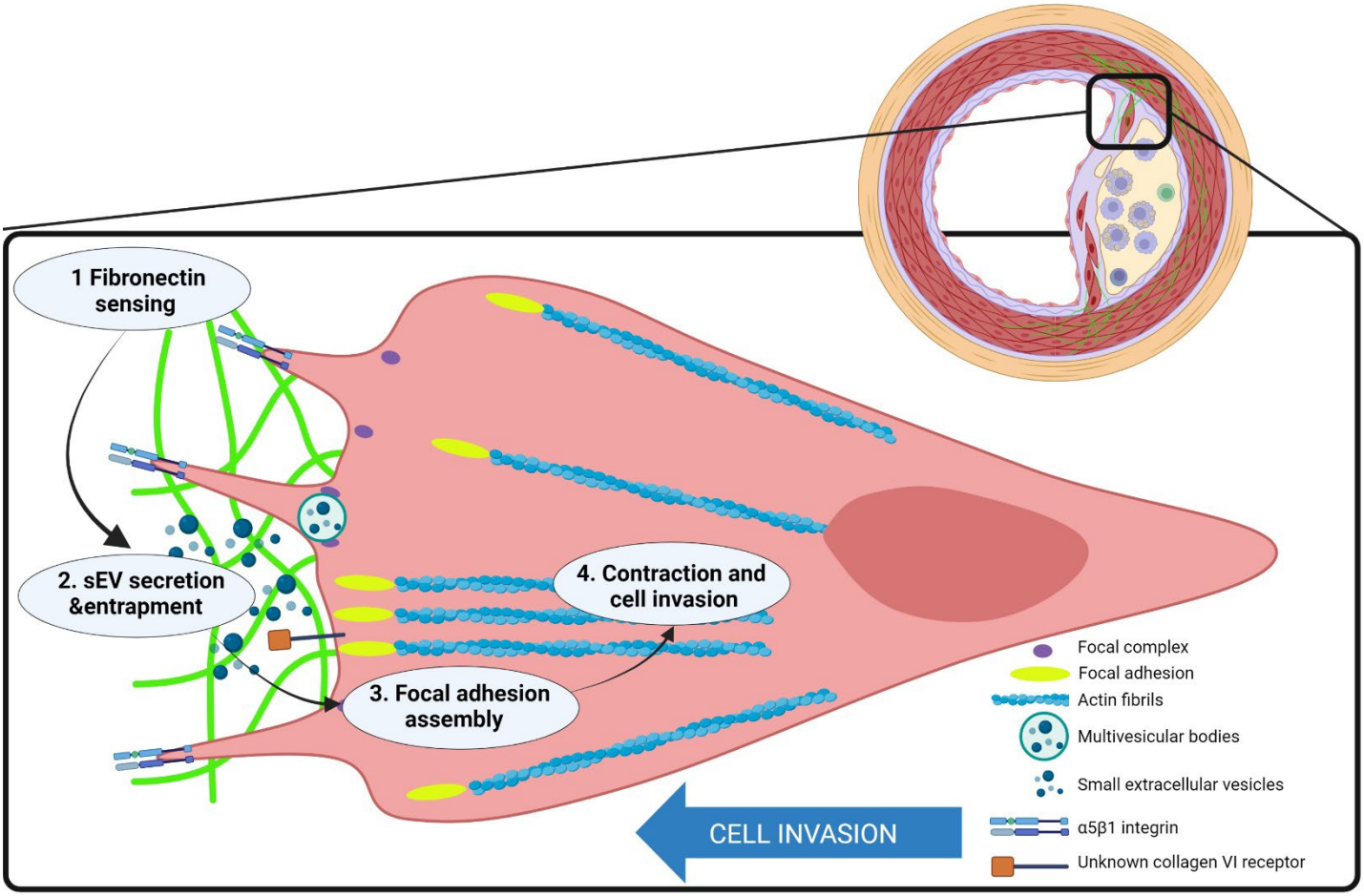

Figure Abstract

Vascular smooth muscle cells sense fibronectin via β1 integrin and secrete small extracellular vesicles loaded with collagen VI via filopodia-like protrusions. These extracellular vesicles are entrapped in the extracellular matrix and induce formation of peripheral focal adhesions. Focal adhesions anchor extracellular matrix to the actin fibrils in the cell. Contraction of the actin fibrils generates the mechanical force for cell locomotion and invasion through the matrix. This figure was created with BioRender (https://biorender.com/).

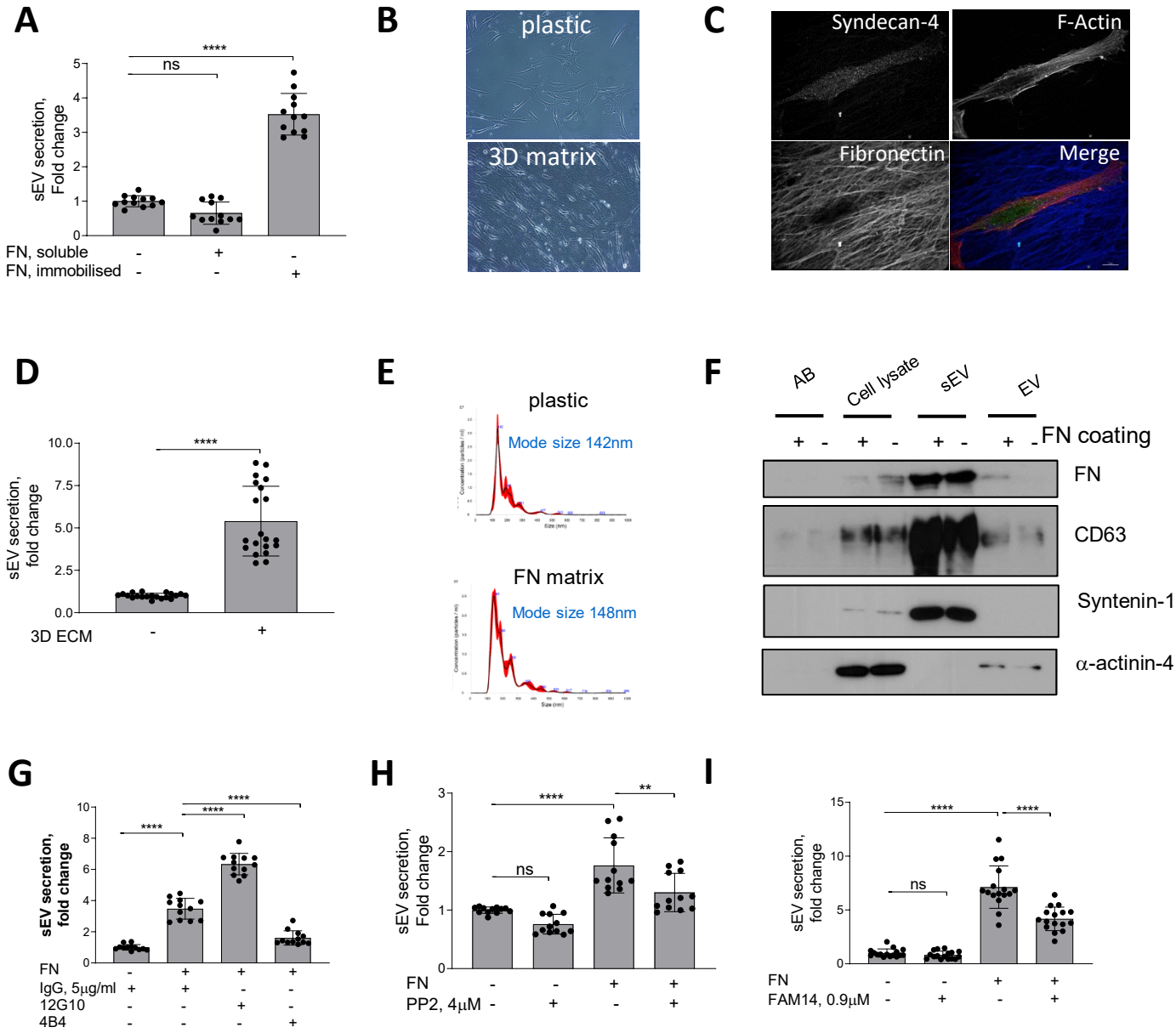

Figure 1. FN matrix stimulates sEV secretion by VSMCs *In Vitro*. **A,** Immobilised FN but not a soluble FN promotes sEV secretion. Cells were cultured for 24h and sEVs in conditioned media were measured by CD63-beads assay. N=4 with technical triplicates. ANOVA, ****p<0.0001 **B,** Micrograph showing VSMC plated onto plastic or 3D matrix. **C,** VSMCs were plated on the 3D matrix for 24h, fixed and labelled for Syndecan-4 (green), F-actin (phalloidin, red) and fibronectin (blue) Size bar, 10μm. **D**, 3D matrix promote sEV secretion. Cells were cultured for 24h and conditioned media was collected and sEV secretion was measured by CD63-beads assay. N=3, T-test **E,** FN matrix does not affect sEV mode size. VSMCs were plated on non-coated or FN-coated flasks and incubated for 24h. Isolated sEVs were analysed by Nanoparticle Tracking Analysis. Representative from N=3. **F,** sEV and EV markers distribution is not altered by FN matrix. Cells were plated on non-coated or FN-coated flasks and AB, EV and Apoptotic bodies (AB, 1.2K pellet), extracellular vesicles (EV, 10K pellet) and small extracellular vesicles (sEVs, 100K pellet) were isolated by differential ultracentrifugation and analysed by western blotting. Equal protein load. Representative image from N=3. **G,** FN induces secretion of sEVs by activating β1 integrin. VSMCs were plated on non-coated or FN-coated plates in the absence or presence of integrin activating (12G10) or inhibiting (4B4) antibodies for 24h and conditioned media was analysed by CD63-bead assay. N=3, ANOVA, ****p<0.0001 **H,** Src is required for the sEV secretion. Cells were plated and sEV secretion was measured as in 2A. N=3, ANOVA, **p<0.0001 **I,** Inhibition of FAK blocks FN-induced sEV secretion. Cells were plated and sEV secretion was measured as in 1A. N=3, ANOVA

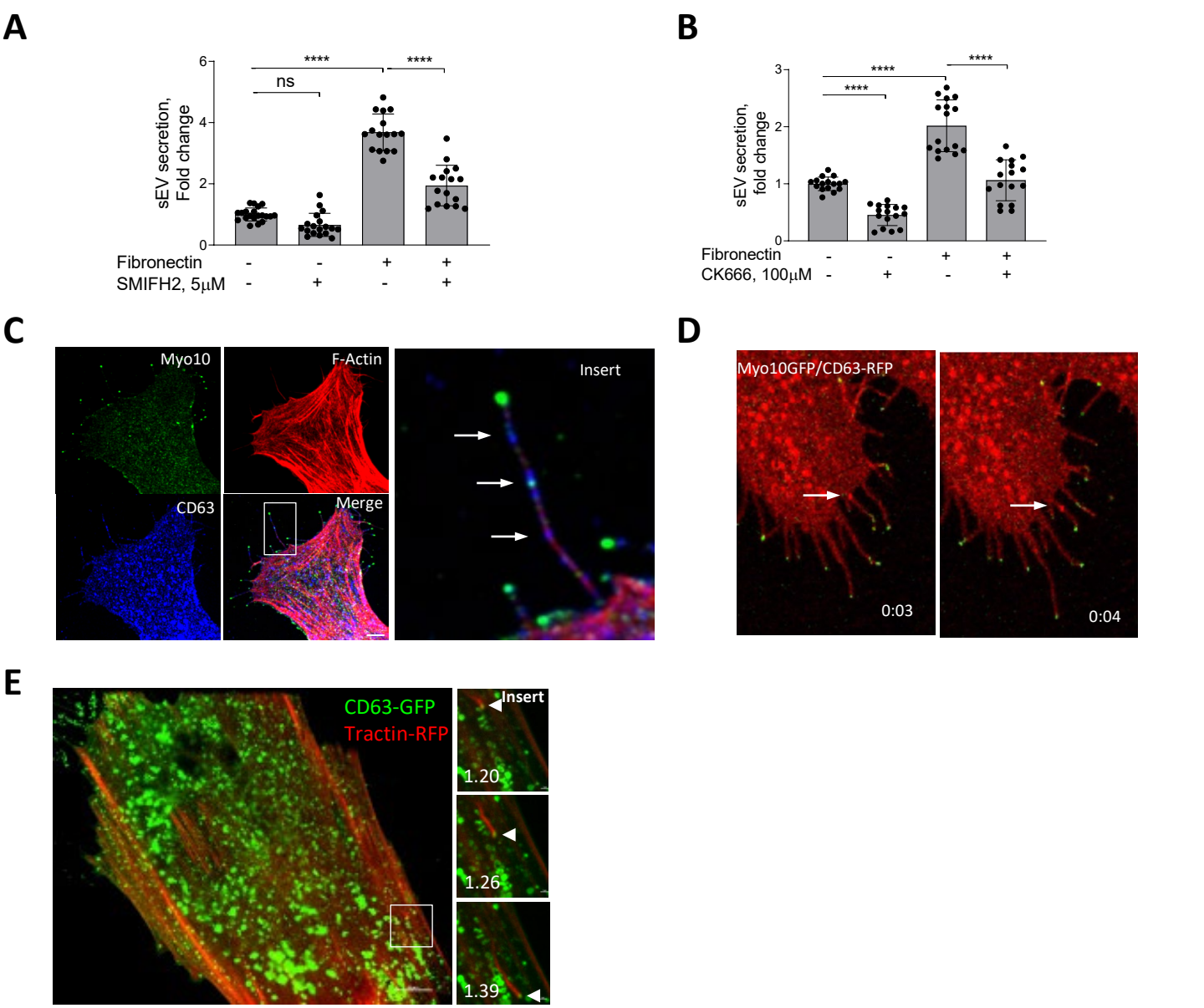

Figure 2. sEV secretion depends in branched actin cytoskeleton and occurs via filopodia.
A, Formin inhibitor, SMIFH2 blocking filopodia formation reduces sEV secretion from FN-plated cells only. Cells were plated onto non-coated or FN-coated plates for 24h and conditioned media was analyzed by CD63-bead assay. N=3, ANOVA **B,** Arp2/3 inhibition with CK666 reduces sEV secretion in VSMC independently on FN plating. Cells were plated onto non-coated or FN-coated plates for 24h and conditioned media was analyzed by CD63-bead assay. N=3, ANOVA **C,** CD63 MVBs (arrows) are detected in filopodia-like structures. VSMCs were plated on FN-coated plate for 24h and cells were stained for Myo10 (green), CD63 (blue), F-actin (phalloidin, red). Size bar, 10μm. **F,** Still images of a time-lapse showing that MVBs are transported to the filopodia tip in the live VSMC. Cells were co-transfected by CD63-RFP and Myo10-GFP, cultured for 24h and time-lapse video was captured using confocal spinning disk microscopy. Snapshots were taken at T=3s and T=4s after start of the video. **E,** Still images of a time-lapse showing that transported MVBs are attached to F-actin tails. VSMCs were co-transfected with CD63-GFP and F-tractin-RFP and time-lapse was captured using confocal spinning-disk microscopy. Arrow head – position of CD63 MVB across time. Time, min. Size bar, 10μm.

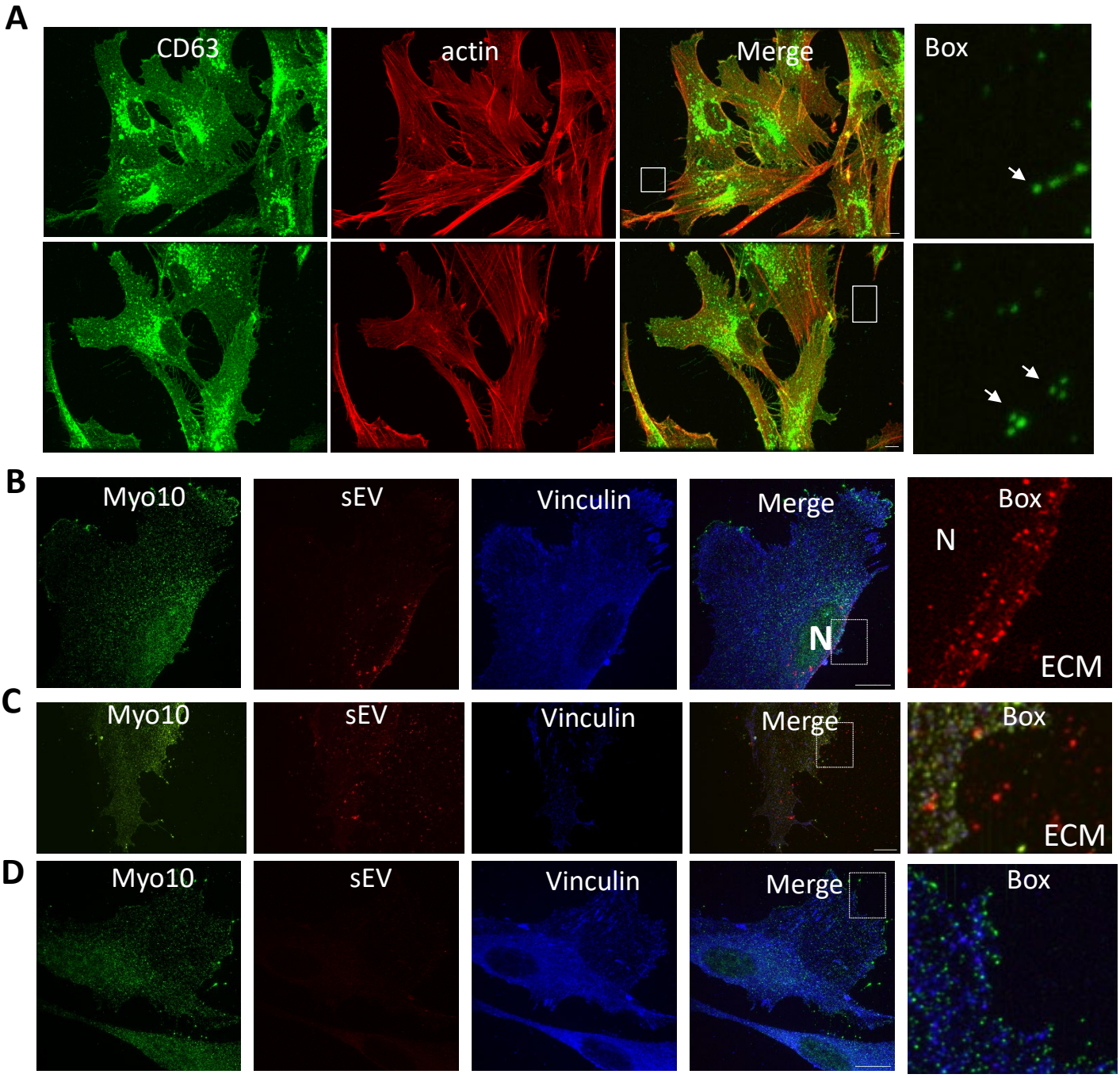

Figure 3. Endogenous and exogenous sEVs are trapped by ECM In Vitro. **A,** VSMC were plated onto dish not coated (top) or coated with FN (bottom) for 24h and stained for the membrane sEV marker, CD63 and actin. Note an accumulation of CD63 puncta in particular in close proximity to filopodia-like cell projectiles. Size bar, 10µm. **B**, VSMC were plated on the FN coated dish and Alexa568-labelled sEV were added to the cell media for 3h. Cells were fixed and stained for filopodia marker Myo10 (green) and vinculin (blue). Note perinuclear localisation of internalised sEVs. Size bar, 10µm. Representative image from N = 3. **C**, VSMC were plated on the FN coated dish pre-coated with Alexa568-labelled sEV and incubated for 24h. Cell staining as in Fig 3B. Note even distribution of sEVs across the matrix and cell area. **D**, VSMC were plated on the FN coated dish in the absence of Alexa568-labelled sEV and incubated for 24h. Cell staining as in Fig 3B. Note the absence of signal in sEV channel.

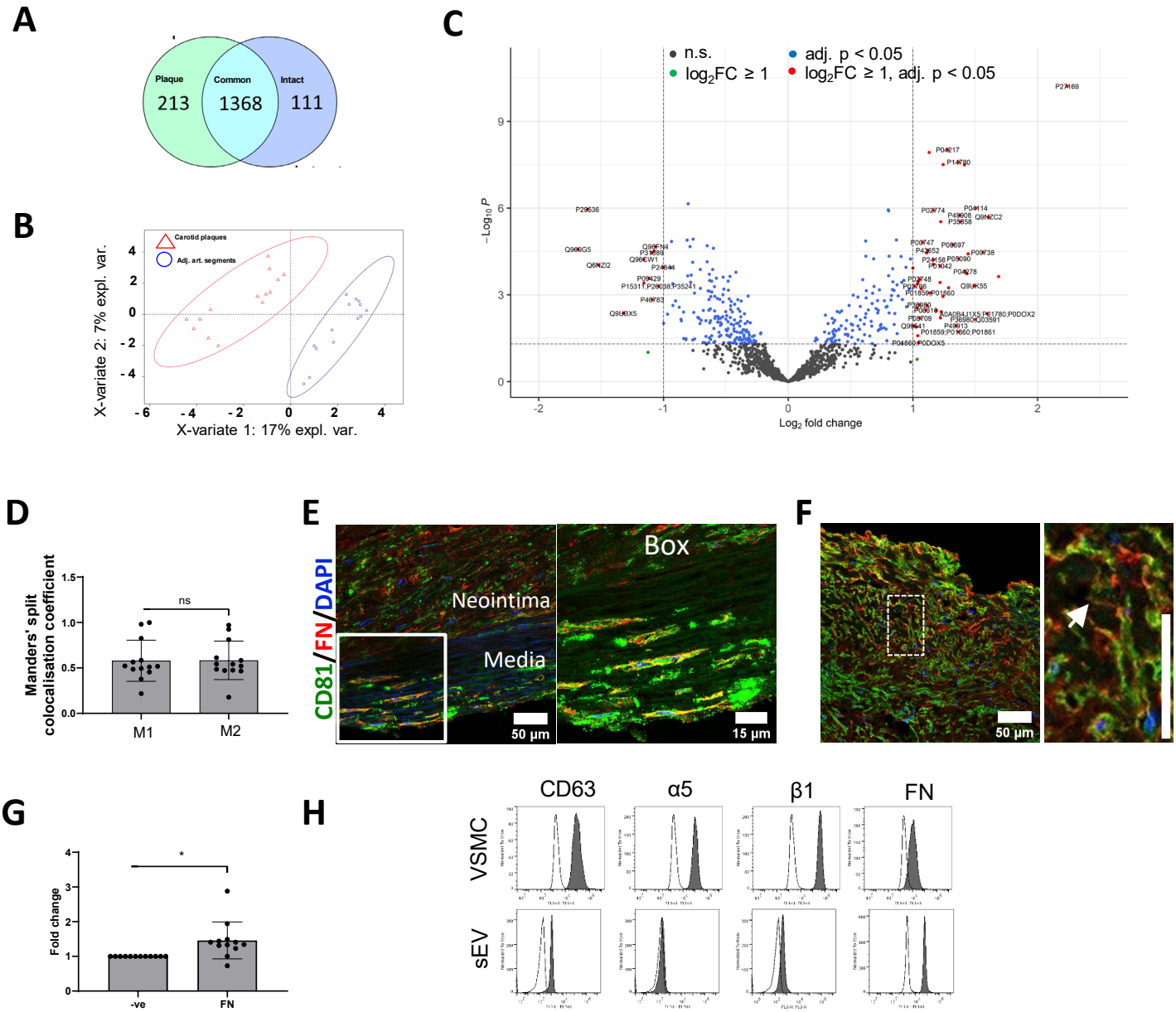

Figure 4. Fibronectin deposition in the atherosclerotic plaque is spatially associated with sEV markers.
A, Proteomic profiling of pairwise collected carotid atherosclerotic plaques and adjacent intact arterial segments. Venn diagram shows the number of plaque-specific (n = 213) and intact-specific (n = 111) proteins as well as the number of proteins which are common for both vascular regions (1,368). **B**. Partial least-squares discriminant analysis indicates clear classification pattern between the carotid plaques (indicated by red triangles) and adjacent intact arterial segments (indicated by blue circles). N = 14. **C**. Volcano plot illustrates that 46 proteins are significantly overexpressed in plaques whilst 13 proteins are significantly upregulated in adjacent intact arterial segments. **D**, Manders' split colocalization coefficient for the overlap of FN with CD81 (M1) and CD81 with FN (M2). Neointima region as in Fig. 4E. **E**, Atherosclerotic plaques were co-stained for fibronectin (FN) and sEV marker, CD81. Cell nuclei were counterstained with DAPI. Main figure: x200 magnification, size bar, 50 µm. Box: x400 magnification, size bar, 15µm. Note an accumulation of FN in the neointima. **F,** Spatial distribution of FN and CD81 in the neointima. Note high overlap between FN and CD81 in the extracellular matrix. x200 magnification, size bar, 50 µm. **G,** Quantification of FN content in atherosclerotic plaques. Samples were analysed by western blot and bands intensity was quantified in ImageJ. Fold change was calculated as ratio of band intensity in the atherosclerotic plaque to band intensity in the adjacent intact arterial segments normalised to GAPDH. Note that FN content is elevated in atherosclerotic plaques relative to the adjacent intact arterial segments. Paired t-test. **H**, FN is presented on the surface of the VSMC-derived sEV along with α5β1 integrin. VSMC sEVs were immobilised on the 4µm beads. sEV-beads and VSMCs were stained with the antibodies (filled graphs) in non-permeabilised conditions and analysed by flow cytometry.

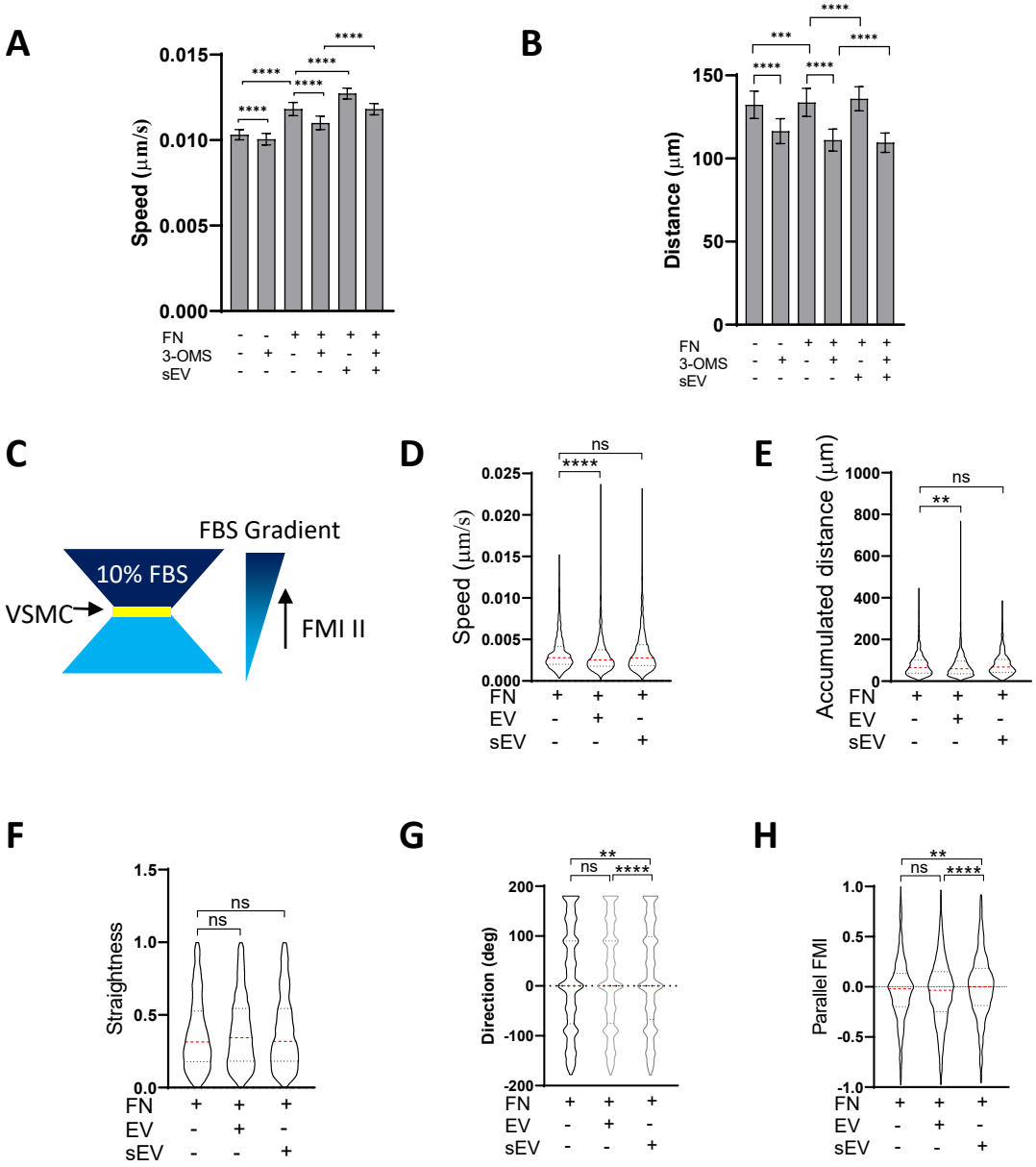

Figure 5. sEV induces directional VSMC invasion. **A, B** VSMC migration in 2D assay. VSMC were plated onto FN in the absence or presence of SMPD3 inhibitor (3'-OMS) and/or sEV (25ug). Cells (n>900) were tracked for 4h. ANOVA, N=3. ****,p<0.0001 **C.** Chemotaxis µ-slide diagram. Yellow, cell chamber, blue chemoattractant-free medium chamber, dark blue – chemoattractant medium chamber. **D-H,** sEV promote directional VSMC invasion. Cells (n=600) were seeded to the FN-enriched Matrigel matrix in µ-Slide Chemotaxis assay and stained with Draq5. Cell tracking was conducted by OperaPhenix microscope for 12h and cell invasion parameters were quantified using Columbus. Kruskal-Wallis test, N=4, **, p<0.01 **I-K,** VSMCs were treated with control siRNA (Scramble) or collagen VI-specific siRNA pools for 24h and cell invasion was measure as in panel G-H, respectively. Kolmogorov-Smirnov test, *, p<0.05

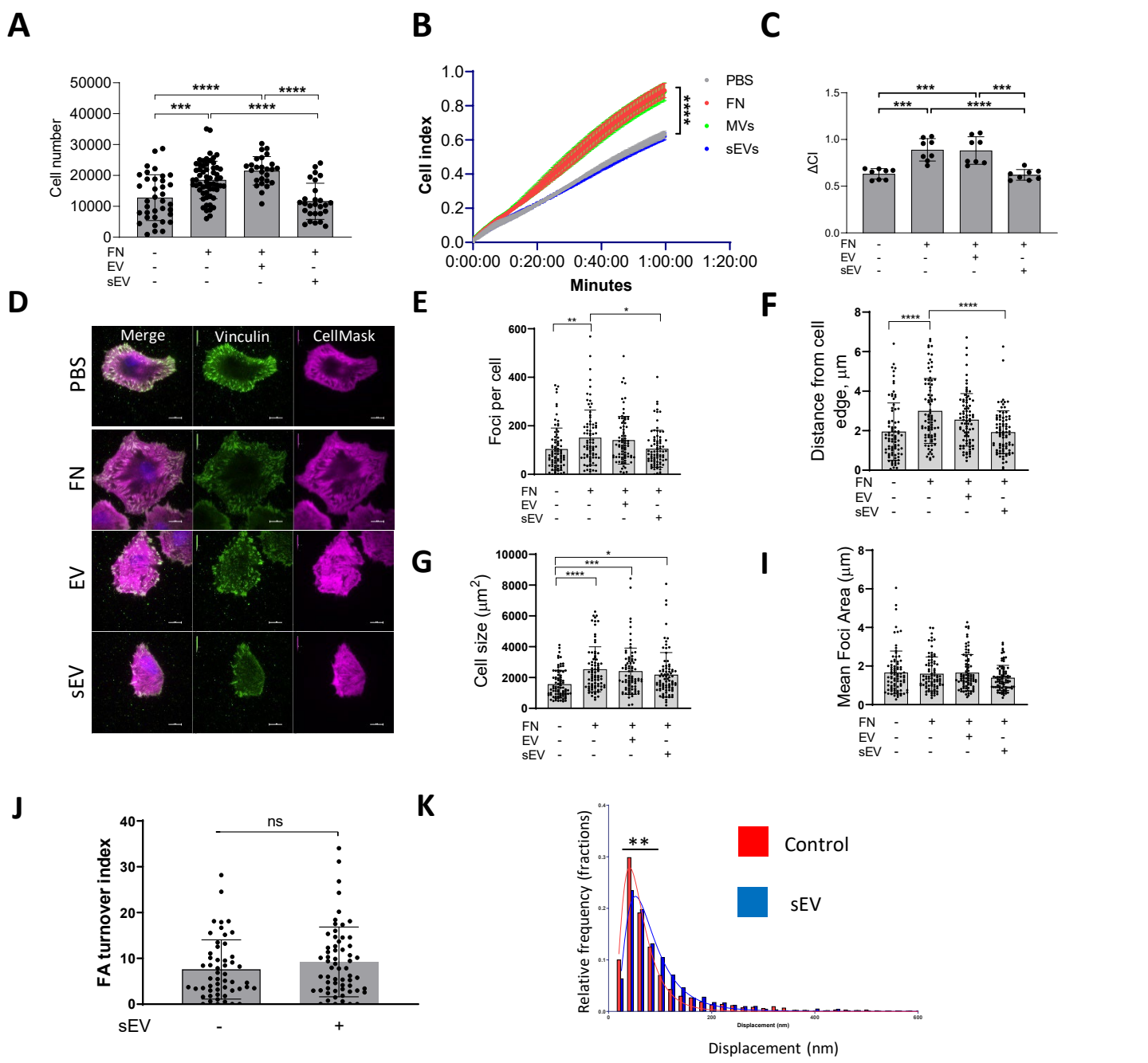

Figure 6. sEV induces formation of peripheral FAs. **A,** VSMC were plated on FN matrix for 30min and adhered cells were counted by crystal violet staining. N=6, ANOVA, ***p<0.001, ****, p<0.0001 **B, C,** VSMC spreading onto FN was tracked by using ACEA's xCELLigence Real-Time Cell Analysis. Note that FN matrix promoted VSMCs adhesion but addition of sEVs inhibited cell spreading. N=3, ANOVA **D,** VSMCs spread onto FN for 30 min and cells were fixed and stained with CellMask (magenta) and vinculin (green). Size bar, 10µm. **E, F, G, I** Quantification of FA number, distance from plasma membrane, cell size and mean FA size per cell, respectively. FA were stained as in 5D and quantified. Representative data from N=3, ANOVA, *p<0.05, **p<0.01. **J,** Focal adhesion turnover is not affected by sEVs. VSMC were transfected with Paxillin-RFP and plated on the FN in the absence or presence of immobilised sEVs. Images were captured for 30min using confocal spinning disk microscopy and FA turnover was quantified using extracted images analysis, N=4, Unpaired T-test. **K,** sEV induces formation of strong-pulling FAs. VSMC transfected with Paxillin-RFP were plated on the PDMS pillars which were covered with FN and sEVs and pillar displacements were quantified**.** **p<0.01, Unpaired T-test, Representative data from N=2.

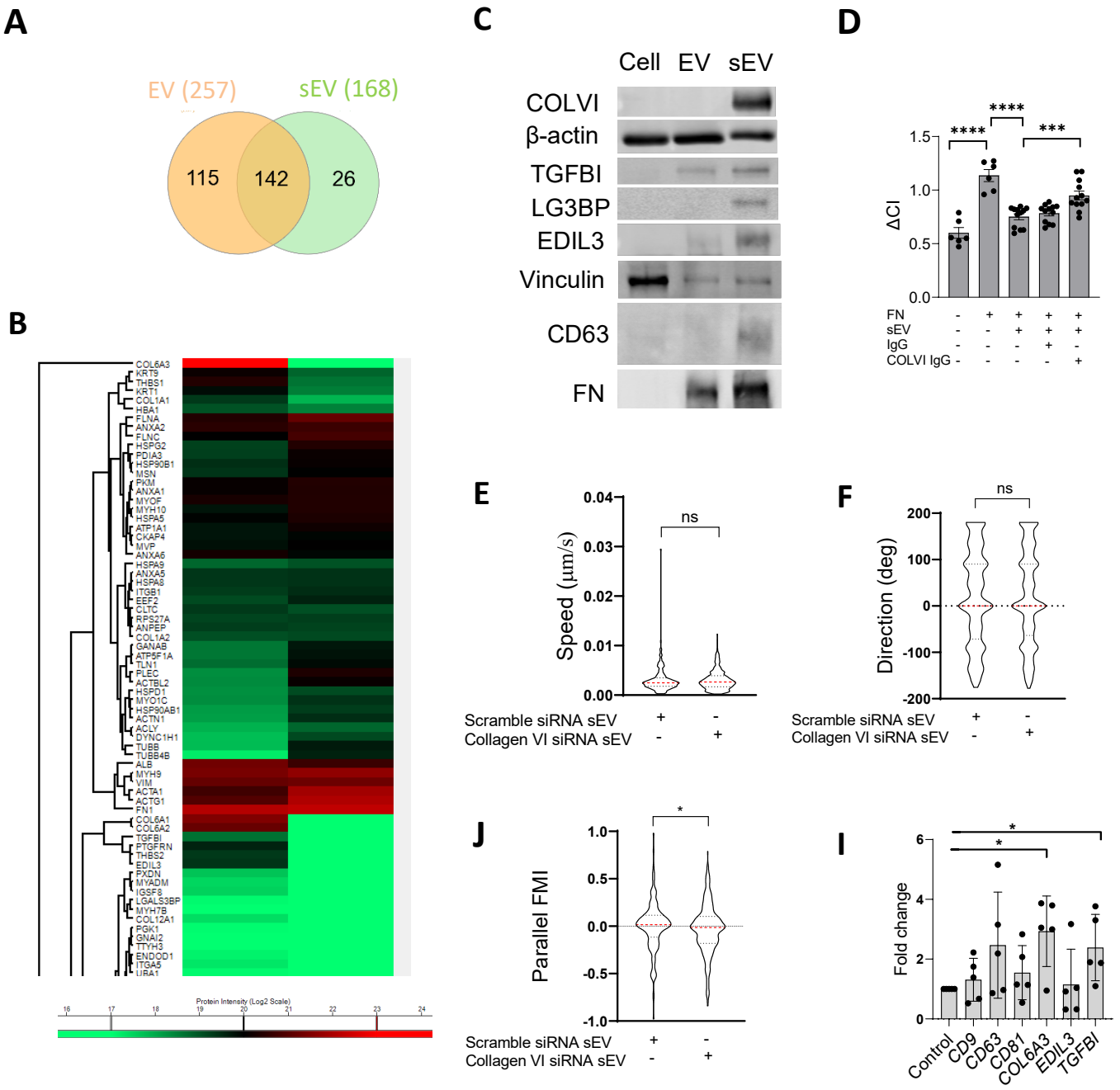

Figure 7. sEVs blocks focal adhesion formation by presenting collagen VI.
A, Proteomic analysis of VSMC-derived sEVs and EV. Venn diagram. N=3. **B,** Protein enrichment in the EV and sEV proteome. Heat Map. N=3. **C,** Western blot validation of sEV cargos. EV and sEV were isolated from VSMC's conditioned media by differential ultracentrifugation and analysed by western blotting. Representative image from N=3. **D,** VSMC adhesion is regulated by collagen VI loaded to sEV. FN matrices were incubated with sEV and anti-collagen VI antibody (COLVI IgG) or control IgG. Cell adhesion was tracked by using ACEA's xCELLigence Real-Time Cell Analysis. ANOVA, N=3. **E, F, J,** sEV promote directional VSMC invasion. VSMCs were treated with control siRNA (Scramble) or collagen VI-specific siRNA pools for 24h and were seeded to the FN-enriched Matrigel matrix in μ-Slide Chemotaxis assay and stained with Draq5. Cell tracking was conducted by OperaPhenix microscope for 12h and cell invasion parameters were quantified using Columbus. Kolmogorov-Smirnov test, *, $p<0.05$ **I**, Real-time PCR analysis of expression of CD9, CD63, CD81, COL6A3, EDIL3 and TGFBI in atherosclerotic plaque. *, $p<0.05$, Paired t-test, N=5.

Supplementary Figures

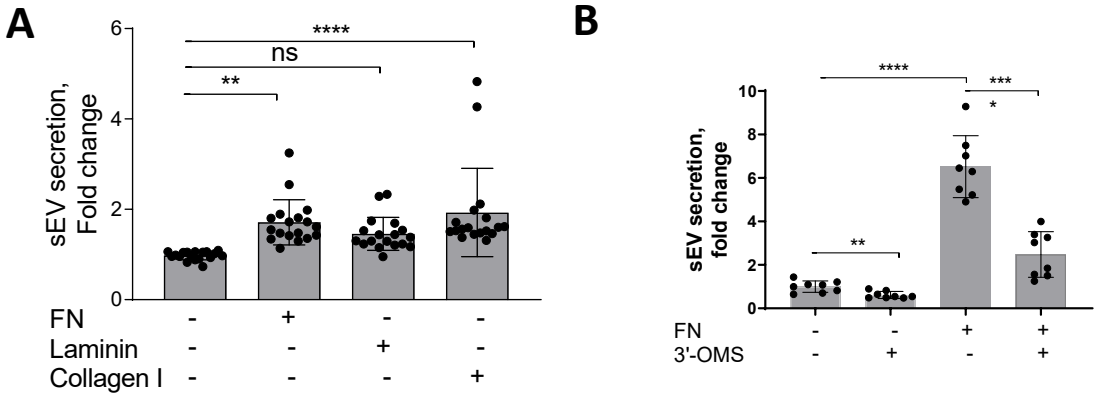

Figure S1. FN matrix stimulates sEV secretion by VSMCs. **A,** FN and collagen I but not laminin stimulate secretion of CD63-enriched exosomes. VSMCs were plated on the various matrices for 24h and sEV secretion was measured by CD63-beads assay. N=3, ANOVA **p<0.01 **B,** Inhibition of SMPD3 blocks sEV secretion by VSMC plated onto FN matrix. VSMCs were plated on non-coated or FN-coated plates for 24h and conditioned media was analysed by CD63-bead assay. N=2 with n=4 for each, ANOVA, ***, p<0.001, ****p<0.0001

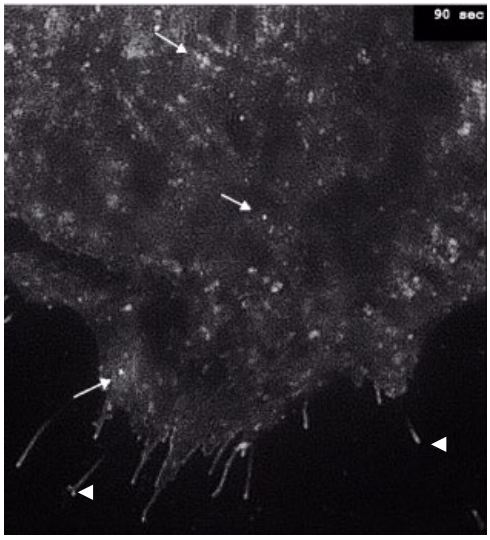

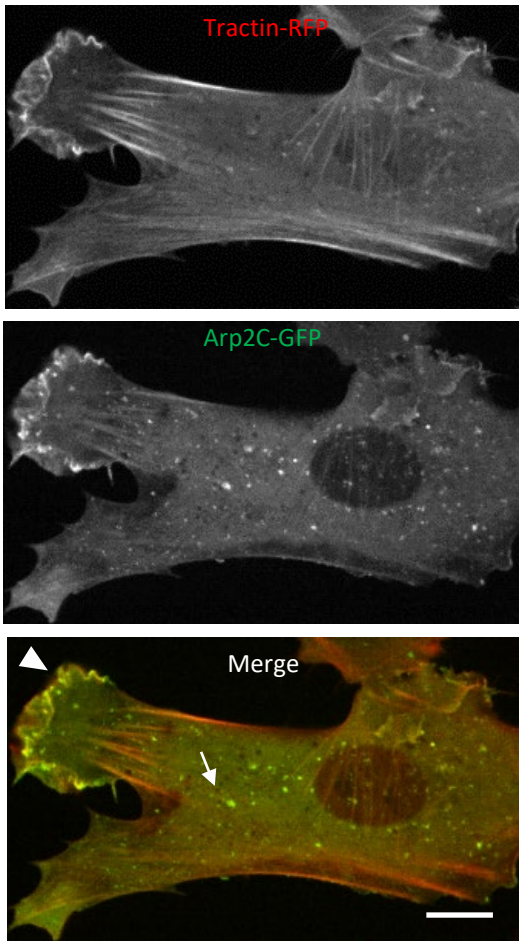

Supplementary Figure S2 A, sEV secretion detected with CD63-pHluorin. VSMCs were co-transfected with CD63-pHluorin and incubated for 24h. Time-lapse was captured using confocal spinning-disk microscopy. Arrows, typical "burst"-like appearance of sEV secretion at the cell-ECM interface. Arrows, an intense CD63-pHluorin staining along filopodia-like structures indicating that sEV release can occur in filopodia. **B**, Still images of a time-lapse showing that Arp2/3 and F-actin form tails in VSMC cytosol. VSMCs were co-transfected by ARPC2–GFP and F-tractin-RFP and cultured for 24h. Time-lapse video was captured using confocal spinning disk microscopy. Note, that Arp2/3 and F-actin are observed in lamellipodia but also detected in the cytosol with the unknown activity (*arrow*). Size bar, 10µm

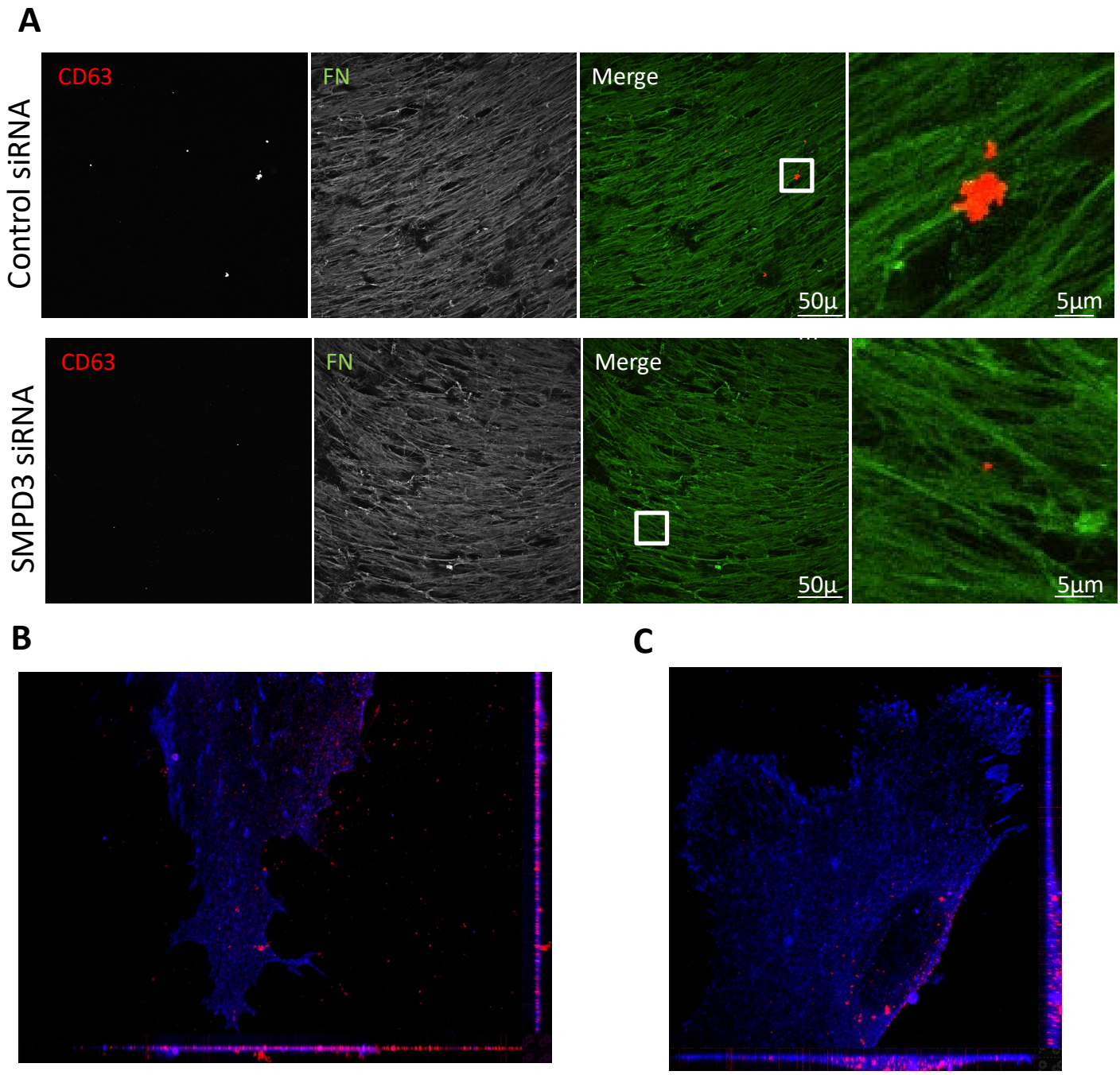

Figure S3 SMPD3-dependent sEVs are trapped in ECM. A. VSMCs were plated onto gelatin-covered plates and treated with control or SMPD3 siRNA for 72 hrs. 3D matrices were generated as described in "Materials and methods" and stained for CD63 and fibronectin. Images were acquired using Nikon AX inverted confocal microscope. Oil 60x Objective. Note the decrease in CD63-positive sEVs associated with the FN fibrils.
B. VSMC were plated on the FN-coated dish and Alexa568-labelled sEV were added to the cell media for 3 h. Cells were fixed and stained for filopodia marker Myo10 (green) and vinculin (blue). Note perinuclear localisation of internalised sEVs. Size bar, 10µm. 3D projection. Myo10 staining channel is removed. Representative image from N=3. **C**, VSMC were plated on the FN-coated dish pre-coated with Alexa568-labelled sEV and incubated for 24h. Cell staining as in Fig 3B. Note even distribution of sEVs across the extracellular matrix and cell area.

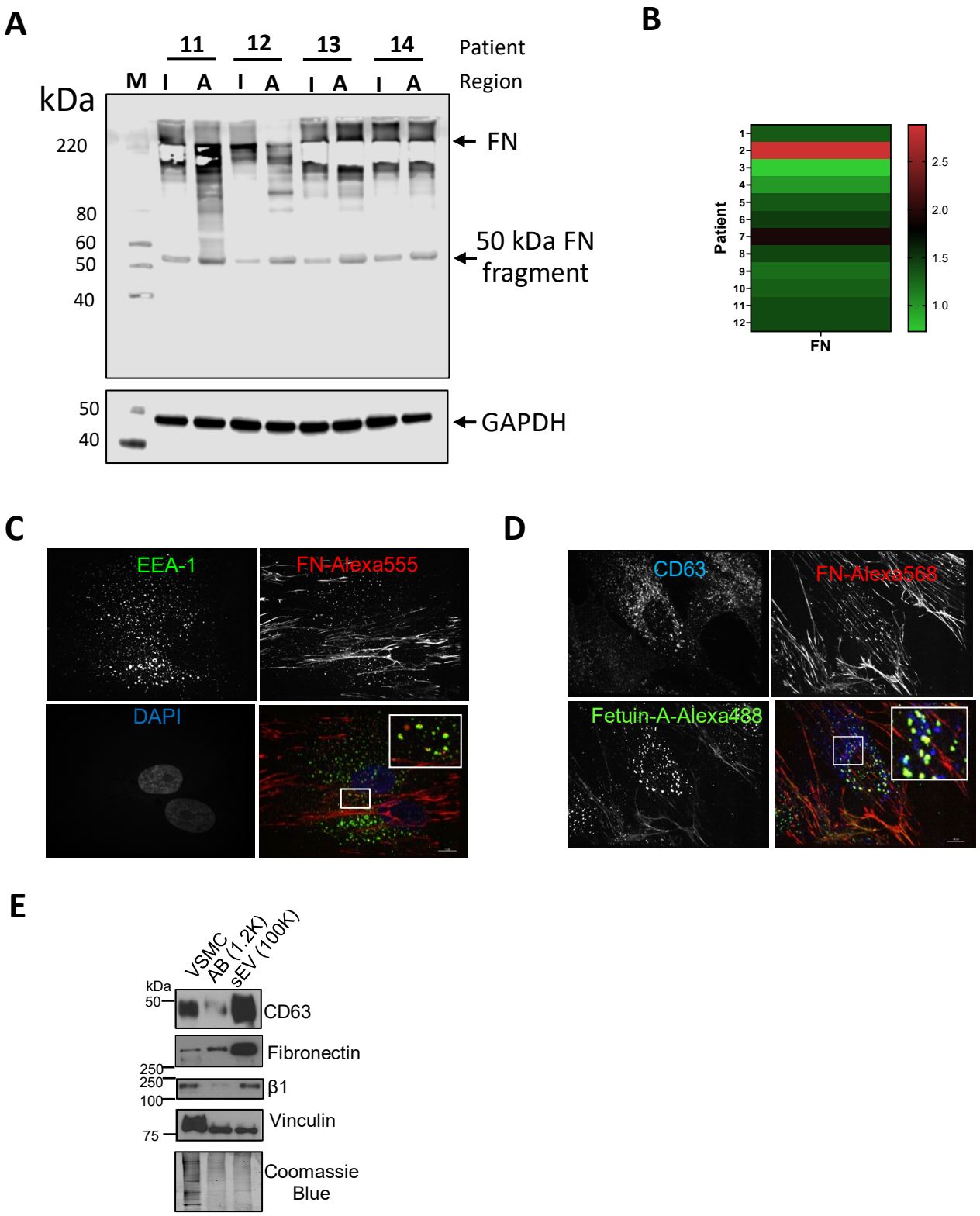

Figure S4. Fibronectin deposition in the atherosclerotic plaque is spatially associated with sEV marker CD81. A. Expression of FN in atherosclerotic plaques. Atherosclerotic plaques (A) and adjacent intact arterial segments (I) were homogenised and analysed by Western blotting. FN is abundantly presented in both regions and 50 kDa FN fragment (Homandberg et al., 1992) intensity was used to quantify FN amount. Representative image for N=4 **B**. Quantification of FN content in atherosclerotic plaques. Heatmap for figure S4A. **D, E,** Exogenously added FN-Alexa555 can be detected in the early endosomes and MVBs. VSMC were incubated with FN-Alexa555 for 30min (D) or 3h (E) and stained for EEA-1 (D, green) or CD63 (E, blue). Size bar, 10um, **F,** FN is presented in sEV along with β1 integrin. Western blot analysis of isolated VSMC-derived sEVs.

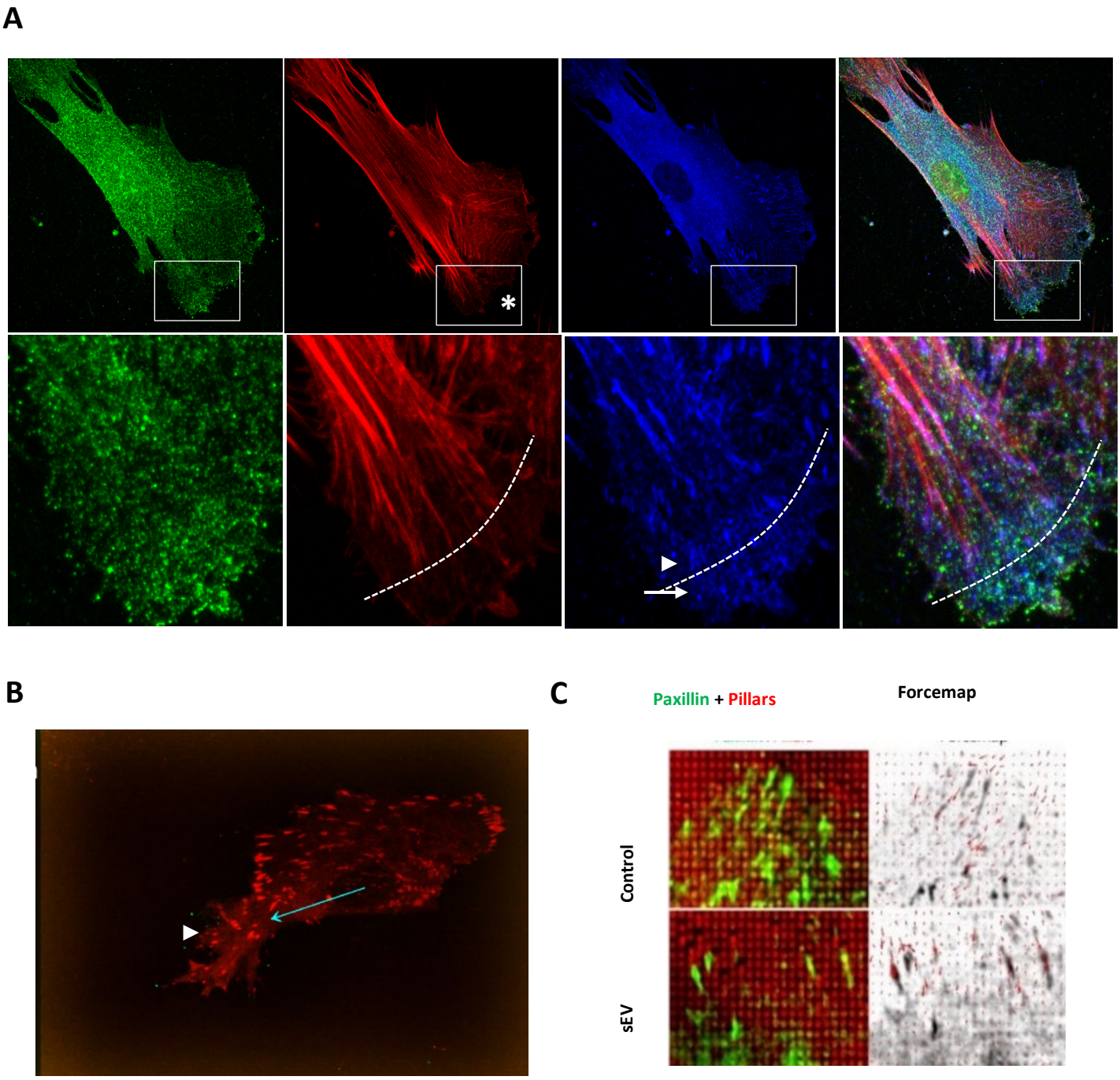

Supplementary Figure S5 sEVs regulate VSMC motility and invasion. A, Centripetal FAs are linked to actin stress fibers. VSMCs were plated on FN-coated plate for 24h and cells were stained for Myo10 (green), CD63 (blue) and F-actin (phalloidin, red). Note the dot-like focal complexes in lamellipodium which are not associated with the contractile actin bundles (arrow) and an appearance of elongated FAs associated with the mature actin bundles (arrowhead). Dotted line, approximate position of the lamellipodium boundaries. Size bar, 10µm. **B,** Mature focal adhesion turnover is not affected by sEVs. VSMC were transfected with Paxillin-RFP and plated on the FN in the absence or presence of immobilised sEVs. Images were captured for 30min using confocal spinning disk microscopy. Note the appearance of the mature FAs in the lamellipodium (Arrowhead). Arrow, direction of the VSMC movement. N=4. **C,** sEV induces formation of FAs with the enhanced pulling force. VSMC transfected with Paxillin-RFP were plated on the PDMS pillars which were covered with FN and sEVs and pillar displacements were quantified**.** Representative image from N=2.

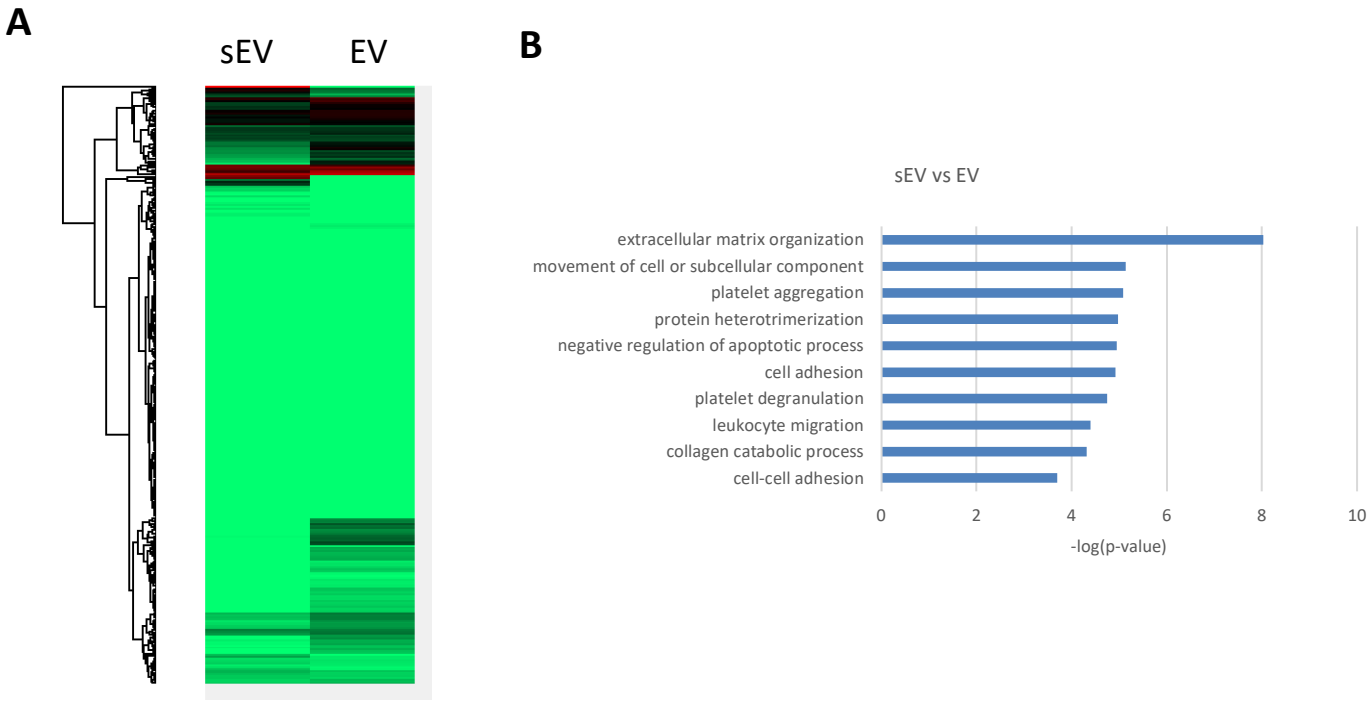

Supplementary Figure S6. Proteomic analysis of VSMC-derived sEVs and EV. VSMC-derived EVs and sEVs were isolated from cells and analyzed by protein mass-spectrometry. N=3. **A.** Clustered proteomic heatmap for EV and sEV. **B,** GO functional enrichment analysis